



# Multiplexed reverse-transcriptase quantitative polymerase chain reaction using plasmonic nanoparticles for point-of-care COVID-19 diagnosis

Nicole R. Blumenfeld<sup>1,2,3</sup>, Michael Anne E. Bolene<sup>1,2,3</sup>, Martin Jaspan<sup>2</sup>, Abigail G. Ayers<sup>1</sup>, Sabin Zarrandikoetxea<sup>1,2</sup>, Juliet Freudman<sup>2</sup>, Nikhil Shah<sup>1,2</sup>, Angela M. Tolwani<sup>1,2</sup>, Yuhang Hu<sup>1,2</sup>, Terry L. Chern<sup>1</sup>, James Rogot<sup>1</sup>, Vira Behnam<sup>1</sup>, Aditya Sekhar<sup>1</sup>, Xinyi Liu<sup>1,2</sup>, Bulent Onalir<sup>1,2</sup>, Robert Kasumi<sup>1</sup>, Abdoulaye Sanogo<sup>1</sup>, Kelia Human<sup>1</sup>, Kasey Murakami<sup>1</sup>, Goutham S. Totapally<sup>1</sup>, Mark Fasciano<sup>2</sup> and Samuel K. Sia<sup>1</sup>✉

**Quantitative polymerase chain reaction (qPCR) offers the capabilities of real-time monitoring of amplified products, fast detection, and quantitation of infectious units, but poses technical hurdles for point-of-care miniaturization compared with end-point polymerase chain reaction. Here we demonstrate plasmonic thermocycling, in which rapid heating of the solution is achieved via infrared excitation of nanoparticles, successfully performing reverse-transcriptase qPCR (RT-qPCR) in a reaction vessel containing polymerase chain reaction chemistry, fluorescent probes and plasmonic nanoparticles. The method could rapidly detect SARS-CoV-2 RNA from human saliva and nasal specimens with 100% sensitivity and 100% specificity, as well as two distinct SARS-CoV-2 variants. The use of small optical components for both thermocycling and multiplexed fluorescence monitoring renders the instrument amenable to point-of-care use. Overall, this study demonstrates that plasmonic nanoparticles with compact optics can be used to achieve real-time and multiplexed RT-qPCR on clinical specimens, towards the goal of rapid and accurate molecular clinical diagnostics in decentralized settings.**

For three decades, polymerase chain reaction (PCR) has served as the gold-standard technique for the detection of nucleic acids from human clinical specimens<sup>1,2</sup>. However, PCR is not commonly performed as a clinical diagnostic at point-of-care (POC) settings, with one limitation being the difficulty and cost of instrumentation for ramping up and down the temperature in a repeated, fast and controlled manner<sup>3–6</sup>. In particular, traditional thermocyclers set the temperature of the reaction vessel using conductive and convective heat transfer from heat blocks that exhibit the Peltier effect; due to large thermal mass and low thermal conductivity of the heat blocks<sup>7</sup>, the thermocycling procedure requires bulky instrumentation and long operation time. These requirements have limited PCR to mainly the laboratory settings, contributing to a scarcity of accurate POC diagnostics and bottlenecks in test results during the COVID-19 pandemic<sup>6,8–11</sup>.

PCR is most commonly offered in the form of quantitative PCR (qPCR), which has transformed clinical diagnostics<sup>12</sup> in allowing amplified products to be detected earlier during a run, and for infectious units to be quantified via cycle threshold (Ct) values. Compared with end-point PCR, the real-time fluorescence monitoring feature of qPCR poses additional technical hurdles for POC miniaturization. Instead of heat blocks, our approach for thermocycling uses direct heating of the solution via plasmonic nanoparticles, in which infrared (IR) radiation interacts with the electrons of nanoparticles to produce oscillation of the electron cloud and subsequent generation of heat; this photothermal method achieves rapid heating of solutions<sup>13</sup> with small optical components.

Although plasmonic heating has been applied for therapeutic<sup>14,15</sup> and molecular diagnostic<sup>16–18</sup> applications, previous work in plasmonic PCR thermocycling has not demonstrated a real-time fluorescence monitoring capability, a central technical feature of qPCR (as opposed to end-point PCR<sup>19</sup>), which is the backbone of laboratory-based PCR methods for clinical diagnostics, including COVID-19 (refs. <sup>20,21</sup>). For example, a previous study on plasmonic thermocycling examined fluorescence at a single wavelength on purified nucleic acids in buffer<sup>16</sup>, and another study used plasmonic heating for end-point PCR rather than qPCR, and did not perform multiplexing within a single sample<sup>22</sup>; further comparison with previous work can be found in Supplementary Tables 1 and 2. A technical limitation to achieve real-time monitoring and qPCR has been fluorescence quenching from nanoparticles. Here we seek to achieve reverse-transcriptase quantitative PCR (RT-qPCR) in a single reaction vessel containing PCR chemistry, fluorescent probes and plasmonic nanoparticles, with the capability of multiplexed fluorescence monitoring during plasmonic thermocycling. We seek to demonstrate RT-qPCR to detect RNA from SARS-CoV-2 from both human saliva and nasal specimens, using small optical components, and more quickly from sample to result than current commercial POC devices (that is, under 30 min).

## Main findings

**Plasmonic RT-PCR with real-time fluorescence monitoring.** We used an optics-driven setup for achieving both thermocycling at IR wavelengths and multispectral fluorescence measurements at visible wavelengths (Fig. 1a). A combination of nanomaterial selection,

<sup>1</sup>Department of Biomedical Engineering, Columbia University, New York, NY, USA. <sup>2</sup>Rover Diagnostics, New York, NY, USA. <sup>3</sup>These authors contributed equally: Nicole R. Blumenfeld, Michael Anne E. Bolene. ✉e-mail: ss2735@columbia.edu

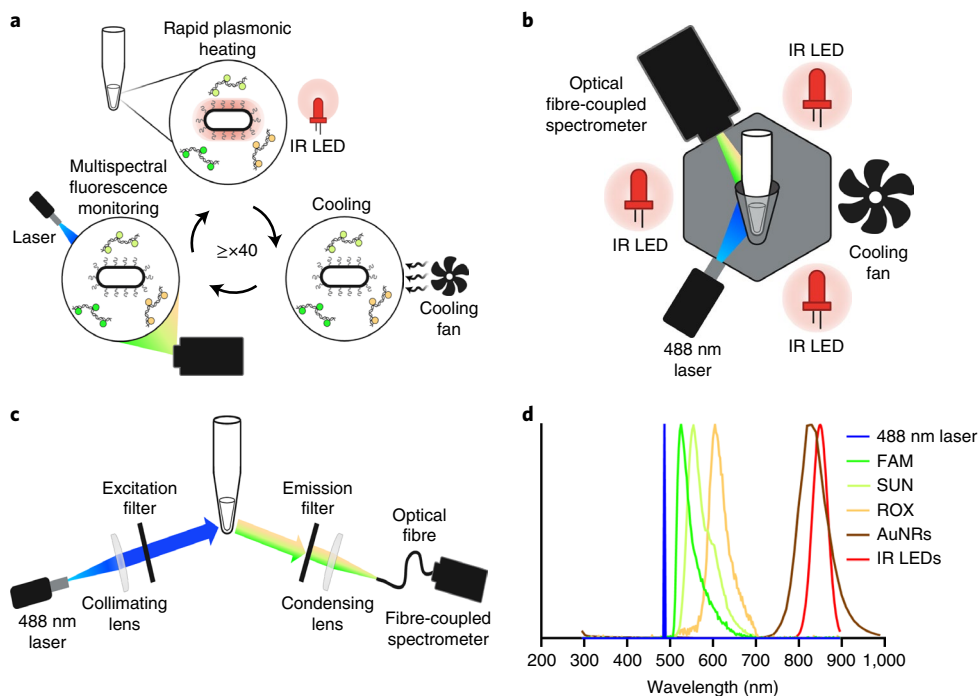


**Fig. 1 | Overall concept and design of multiplexed, real-time plasmonic RT-PCR.** **a**, Schematic of multiplexed real-time plasmonic RT-PCR, with heating driven by IR LEDs acting on AuNRs and cooling aided by a 12 V fan. The AuNRs are suspended in solution in a 0.2 ml PCR tube, rapidly absorbing light from the LEDs and converting it to heat, allowing for fast PCR thermal cycling. A 488 nm laser and spectrometer setup provides real-time fluorescence detection and takes a measurement at the end of each annealing/extension hold. **b**, Schematic of the instrument. A PCR tube is surrounded by low-cost optical components, without Peltier heating elements. The main components of the instrument include a thin-walled PCR tube surrounded by three IR LED modules, a cooling fan, and a 488 nm laser and spectrophotometer setup for fluorescence detection. The three IR LED modules consist of 850 nm IR LEDs attached to heat sinks as well as heat-sink fans and placed concentrically surrounding the PCR tube. Temperature control can be achieved through closed-loop sensing with a wire thermocouple or through contactless open-loop control. **c**, Schematic of the fluorometer system. Light coming from a 488 nm laser passes through a collimating lens and filter before reaching the PCR tube. Light emitted from the tube passes through a condensing lens and a 500 nm edge emission filter (Semrock) before travelling through an optical fibre to reach the spectrometer. **d**, Graph depicting non-overlapping optical spectra of various components within the system, namely, 488 nm excitation peak, three emissions (520, 555 and 610 nm), IR LED excitation and AuNR absorbance.

instrument setup and deconvolution software enabled this capability. First, in the reaction vessels, we used gold nanorods (AuNRs) with localized surface plasmon resonance in the near-infrared range (~850 nm); this wavelength range allowed the use of fluorescent probes for real-time fluorescence detection without the need to remove AuNRs (another study<sup>22</sup> used nanoparticles with the maximum absorption at 535 nm, which overlaps with the emission spectra of many currently used fluorescent probes for PCR). To drive thermocycling, an optical setup consisting of three IR light-emitting diodes (LEDs), operating at 850 nm and concentrically positioned around a thin-walled PCR tube, produced rapid heating throughout the tube compatible with RT-PCR (Fig. 1b and Extended Data Fig. 1a). With previous work on plasmonic heating showing fluorescence quenching by AuNRs<sup>22</sup> and consequently an inability to monitor fluorescence in real time (as a separate mechanical step was needed for each fluorescence recording), we used a concentration of AuNRs that was sufficiently high to achieve the photothermal effect but also would not interfere with fluorescence measurements, to rapidly generate heat throughout the solution (20  $\mu$ l in volume); during each cycle, cooling was achieved with a small 12 V fan (Fig. 1b and Extended Data Fig. 1a). The intensity and time sequence of the LEDs were calibrated using a K-type thermocouple and custom LabVIEW program, which was fed into a second LabVIEW program to automate the tuning of an open-loop control system.

Second, for real-time fluorescence monitoring, we excited and detected up to three fluorescent probes (FAM, SUN and ROX)

with a common excitation source and detection source (Fig. 1c,d). In particular, with plasmon resonance of AuNRs at near-infrared wavelength, we used a fluorescence setup consisting of a 488 nm laser diode as the excitation source and an optical-fibre-coupled spectrometer that could detect multiple wavelengths (Fig. 1d). A series of collimating lenses, bandpass filter and condensing lens was employed (Extended Data Figs. 1 and 2). Overall, this fluorescence setup uses small components, with a total cost of goods less than US \$1,000 at scale (with the spectrometer being the most expensive component), to achieve real-time multispectral fluorescence monitoring alongside plasmonic thermocycling.

We first demonstrated fast thermocycling using this method of optics-based heating. We used a K-type wire thermocouple inserted in the reaction vessel to measure the temperature, and incorporated proportional–integral–derivative control in a LabVIEW-based thermocycling program for precise temperature settings. This setup achieved amplification with initial temperature holds for 2 min for reverse transcription and 10 s for denaturation, followed by 45 cycles of rapid thermocycling, in less than 15 min total (Fig. 2a). Across the 45 cycles of thermocycling, the setup achieved a heating rate of  $6.7 \pm 0.2 \text{ }^{\circ}\text{C s}^{-1}$  and cooling rate of  $-4.7 \pm 0.1 \text{ }^{\circ}\text{C s}^{-1}$  (Fig. 2b). Next, we assessed the ability to perform RT-PCR via the fluorescence detection of amplified products from a template of purified SARS-CoV-2 RNA in buffer. Via end-point RT-PCR as assessed by a plate reader, for both N1 and N2 primer sets, the method achieved significantly amplified products compared with a negative template

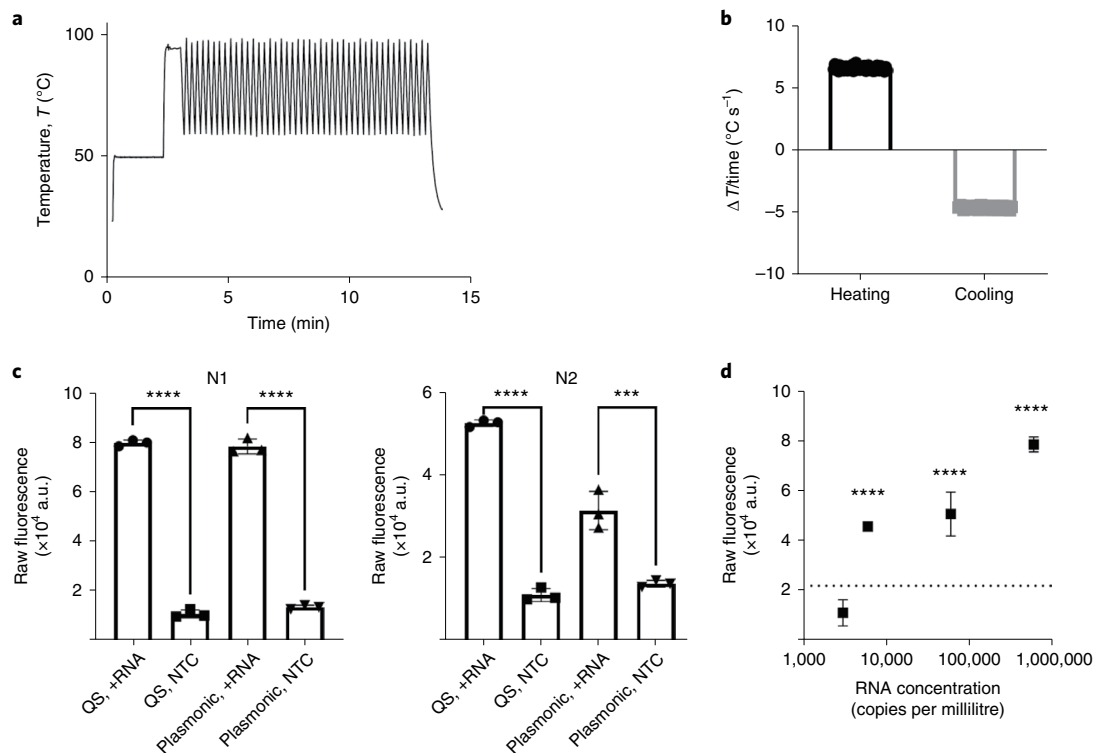


**Fig. 2 | Achievement of fast, multiplexed, plasmonic RT-PCR.** **a**, Well-controlled temperature sequence showing full RT-PCR in <15 min. Cycling parameters consisted of 2 min at 50 °C, 10 s at 95 °C, and 45 cycles between 60 and 95 °C with no holds. **b**, Consistent heating and cooling rates achieved throughout the 45 cycles in the data shown in **a**, with an average heating rate of  $6.7 \pm 0.2 \text{ }^{\circ}\text{C s}^{-1}$  and an average cooling rate of  $-4.7 \pm 0.1 \text{ }^{\circ}\text{C s}^{-1}$  (mean  $\pm$  standard deviation (s.d.),  $n=45$ ). **c**, Initial positive amplification results using our plasmonic RT-PCR system as measured by end-point fluorescence on a plate reader. SARS-CoV-2-purified RNA in buffer was tested at a concentration of  $5.9 \times 10^5$  copies per millilitre ( $n=3$  replicates per condition). Data are presented as mean  $\pm$  s.d. \*\*\*\* indicates adjusted  $p < 0.0001$ , \*\*\* indicates  $p = 0.0001$  and ns indicates 'no significance' as determined by one-way analysis of variance (ANOVA) followed by Tukey's multiple comparison tests. **d**, Initial photothermal amplification LoD data using purified RNA and fast amplification (<16 min). The threshold was determined by running three NTCs and taking the mean plus ten times the standard deviation (dotted line). All the concentrations were run in triplicate or more ( $n \geq 3$ ). Data are presented as mean  $\pm$  s.d. Raw fluorescence for each concentration was compared with the NTC value via one-way ANOVA followed by Sidak's multiple comparisons test and determined to be statistically significant (\*\*\*\* indicates adjusted  $p < 0.0001$ ).

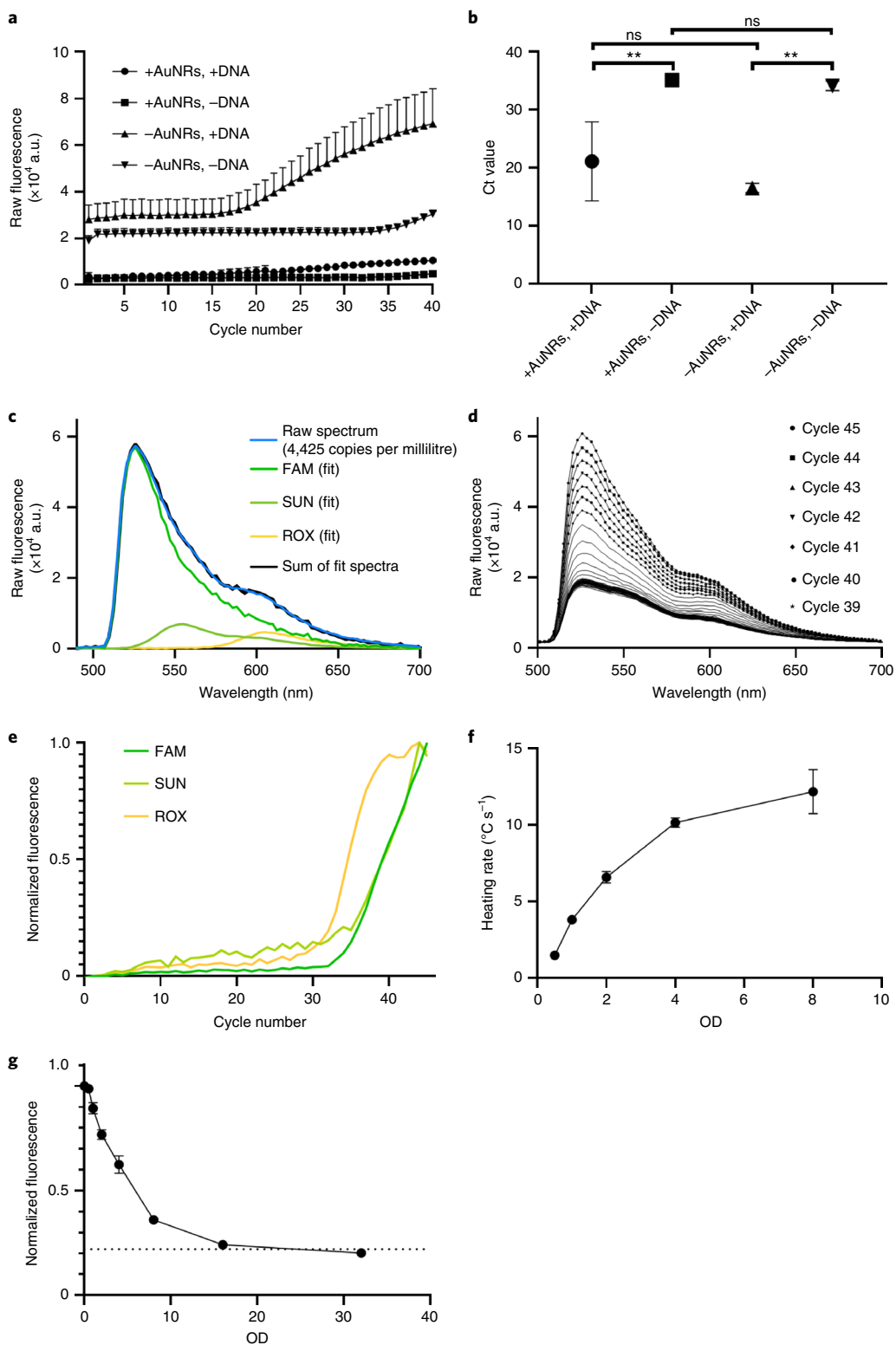
control (NTC) (Fig. 2c). Human ribonuclease P (RP) was amplified as an internal-sample-processing control for all the reactions, as expected. This proof-of-concept experiment produced a limit of detection (LoD) of  $5.9 \times 10^3$  copies per millilitre in less than 16 min (Fig. 2d). Further, we sought to demonstrate plasmonic RT-PCR on human saliva, a specimen matrix of clinical interest for POC diagnostics, including that for COVID-19 (ref. <sup>23</sup>). Specifically, we tested 14 human saliva specimens collected from symptomatic patients (using a setup with two LEDs) and found a sensitivity of 100% and specificity of 100%, compared with laboratory-based PCR (Extended Data Fig. 3). Although this set of experiments used a plate reader for end-point fluorescence measurements, this setup demonstrated the potential for an optics-based method for rapid, extraction-free, plasmonic RT-PCR from SARS-CoV-2 RNA targets, including those from human clinical specimens.

Next, we integrated a multispectral fluorescence detector into the IR thermocycling setup to detect fluorescence signals generated by molecular probes in real time. For fluorescence excitation, we used a high-powered, single-colour laser diode, and for multicolour detection, we used a collimating lens, an optical fibre and a spectrometer; a microcontroller was programmed to take measurements at the end of each cycle (Methods). Due to the known quenching of fluorescence by AuNRs<sup>22,24</sup>, we first sought to investigate the potential interference of AuNRs in the reaction vessel with fluorescence during a PCR process. In a proof-of-concept PCR reaction driven by a

laboratory-based, real-time thermocycler, we observed that despite some fluorescence quenching in the presence of AuNRs, fluorescence could still be effectively monitored over the duration of a full qPCR amplification process (for amplifying spiked SARS-CoV-2 DNA plasmids in human saliva) (Fig. 3a). Quantitatively, the Ct values calculated from fluorescence in the presence of AuNRs were unaffected compared with the Ct values calculated in their absence (Fig. 3b).

With these observations, we characterized our multispectral fluorescence detector setup. The full wavelength spectra collected by the spectrometer allowed for deconvolution via a custom-written algorithm. Based on amplification in our system and fluorescence measurements of individual targets, we were able to deconvolve the full spectra into individual peaks, which allowed the simultaneous detection of three nucleic-acid targets with three real-time probes tagged with FAM, SUN and ROX dyes (Fig. 3c).

We then sought to modify the software to enable real-time fluorescence monitoring by triggering the laser and spectrometer after each amplification cycle. Monitoring the fluorescence of FAM, SUN and ROX in spiked human saliva specimens, we were able to clearly see the amplitude of the spectra increasing with each cycle over time, indicating the potential to perform multiplexed real-time RT-PCR (Fig. 3d). Plotting these data against cycle number confirmed the ability to obtain amplification curves and Ct values, simultaneously for three fluorophores, in real time (Fig. 3e).



**Heating and quenching by AuNRs.** To further characterize AuNR fluorescence quenching and validate our AuNR concentration selection, we tested the effect of AuNR optical density (OD) on the heating rate and fluorescence monitoring. Heating rate for varying AuNR ODs was used to identify the minimum concentration needed to cause temperature changes in the expected period of time. Concentrations lower than the system choice, that is, OD of 2, demonstrated unacceptably slow heating rates that sacrifice rapid

PCR performance, whereas increasing the concentration increases the heating rate nonlinearly and starts to level off at a limit near  $13\text{ }^{\circ}\text{C s}^{-1}$  (Fig. 3f). AuNRs with OD of 2 demonstrated a heating rate of  $6.5\text{ }^{\circ}\text{C s}^{-1}$ . We then tested the limitations of AuNR concentration on fluorescence quenching; higher AuNR concentrations decreased the normalized fluorescence intensity readout, but concentrations far above the OD of 2 remain within the fluorometer's LoD (Fig. 3g). Combined with the results showing fluorescence and Ct values

**Fig. 3 | Integration of real-time fluorescence detection without removal of AuNRs.** Integration with onboard spectrometer, characterization of AuNR OD effect on heating and fluorescence, and analytical characterization of integrated fast RT-PCR amplification of inactivated SARS-CoV-2 virus spiked in patient saliva. **a**, Addition of AuNRs (OD of 18) to RT-PCR reactions quenches the raw fluorescence signal as shown by plotting raw fluorescence as a function of cycle number from reactions on the QuantStudio instrument. 2019-nCoV-N-positive control plasmids (from IDT) were used. **b**, Despite quenching, the Ct values for the data in **a** remain unaffected with and without AuNRs. One-way ANOVA followed by Sidak's multiple comparisons test was performed, where \*\* indicates adjusted  $p < 0.01$  and ns indicates no statistical significance ( $n = 3$  per condition). For the reactions containing AuNRs, the significance was  $p = 0.0066$ . For the reactions without AuNRs, the significance was  $p = 0.0015$ . **c**, Multispectral detection was achieved using a single excitation laser and a spectrometer, and multiple linear regression for spectral deconvolution. N1 amplification is detected via FAM, N2 via SUN and RP via ROX. **d**, Real-time amplification and detection as shown through all the three raw spectral curves increasing over time. **e**, Deconvolved fluorescence values (for three individual targets/colours) against cycle number to calculate the Ct values (Methods provides the Ct value calculations). **f**, Effect of AuNR OD on the heating rate. Heating rate ( $^{\circ}\text{C s}^{-1}$ ) increases for increasing ODs of AuNRs ( $n = 40$  for each concentration). **g**, Effect of AuNR OD on fluorescence monitoring. Normalized fluorescence intensity detection decreases for increasing ODs of AuNRs in dyed TE buffer (using a FAM oligonucleotide from IDT) measured with a fluorometer ( $n = 9$  for each concentration). The fluorometer's LoD indicated by the dotted line (calculated with average fluorescence intensity of stock nanoparticles (OD of 94) with no dye plus ten times the standard deviation). Fluorometer values normalized to the average of OD of zero measurements. The data for figures with error bars are presented as mean  $\pm$  s.d.

during amplification (Fig. 3a,b), this confirmed that AuNR quenching at the chosen concentration of OD of 2 does not affect the fluorometer's ability to accurately detect signal changes during PCR amplification.

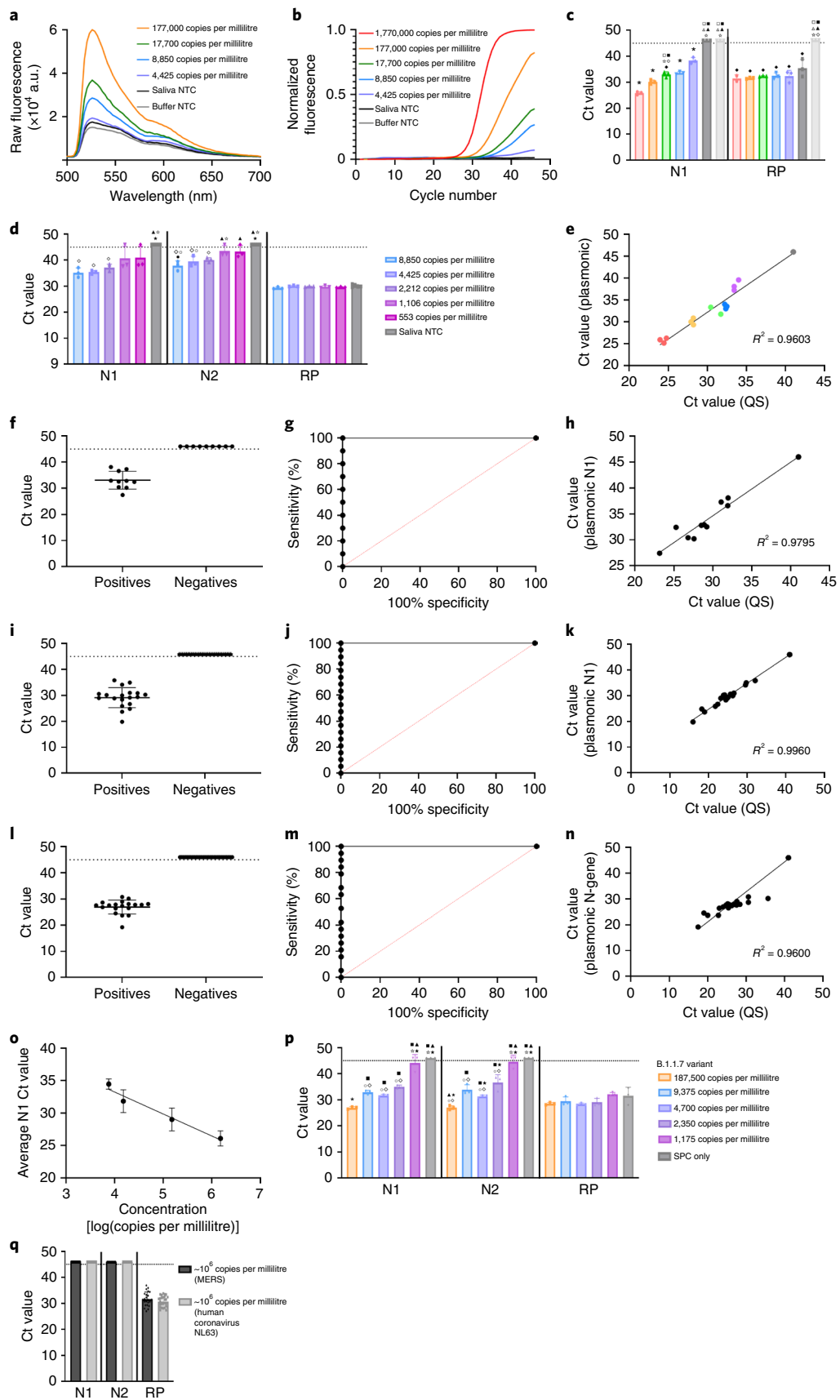
**Testing COVID-19 virus, human samples, variants and related viruses.** We tested the ability of the setup, with integrated plasmonic thermocycling and multispectral fluorescence monitoring, to amplify and detect inactivated SARS-CoV-2 virus particles (BEI Resources) spiked into human saliva at varying viral loads (dilution of specimen with the buffer followed directly by extraction-free RT-PCR has been previously shown to work for nasopharyngeal swabs<sup>25,26</sup> and heat-inactivated saliva samples<sup>27,28</sup>). In an initial proof-of-concept experiment, we measured the end-point fluorescence spectra with our integrated fluorometer. We focused on the detection of the N1 target, as indicated by FAM, as well as the detection of RP, as indicated by ROX. Using virus concentrations ranging from ~180,000 to ~4,000 copies per millilitre in human saliva as positive samples (within the range of SARS-CoV-2 virus exhibited in saliva of most patients<sup>29,30</sup>), the fluorescence values of runs performed on positive samples were clearly distinguishable from those run on samples without templates (NTCs), with the end-point fluorescence signals across the spectra to be proportional to the amount of starting virus in the sample (Fig. 4a).

Next, we performed real-time monitoring in our integrated plasmonic RT-PCR instrument, testing inactivated SARS-CoV-2 virus spiked into human saliva. The average run time, including all the steps of RT-PCR thermocycling, was  $17.9 \pm 0.1$  min. The real-time setup could successfully detect virus concentrations

as low as 4,425 copies per millilitre (Fig. 4b) (which is within the clinically relevant viral load range in saliva for most COVID-19 human subjects<sup>29,30</sup>). Towards quantitation, for the control, Ct values for human RP were similar across different concentrations of spiked SARS-CoV-2 in saliva, which was different from buffer NTC (Fig. 4c, right). By comparison, log-fold differences in copy numbers produced smaller Ct values as virus concentrations increased, as expected (Fig. 4c, left), and both saliva NTCs and buffer NTCs were not detected. In addition, we analysed spiked saliva specimens with the addition of N2 (to N1 and RP), and saw a similar LoD of 2,212 copies per millilitre (testing concentrations below the previous lowest LoD value confirmed a trend towards loss of signal past 2,212 copies per millilitre (Fig. 4d)). Further analysing the quantitative capability of plasmonic RT-qPCR, we compared the Ct values (for viral N1 detection) from varying concentrations with those samples run on a laboratory-based PCR. The Ct values for the two approaches exhibited a coefficient of determination of 0.9603, further demonstrating the potential for quantitative analysis in our instrument (Fig. 4e).

We tested 19 human saliva specimens (ten positives and nine negatives) on the integrated setup with plasmonic thermocycling and real-time fluorescence monitoring. The runs took  $21.0 \pm 1.1$  min. The setup yielded a sensitivity of 100% and specificity of 100% (Fig. 4f), and an area under the curve of 1.0 (Fig. 4g) compared with the reference of laboratory-based PCR. We also evaluated the quantitative capability of the setup. The Ct values obtained in this setup exhibited a coefficient of determination of 0.9795 compared with the Ct values of the same samples run on a laboratory-based PCR instrument (Fig. 4h). Past studies have placed Ct values into

**Fig. 4 | Multiplexed plasmonic RT-qPCR for detection of SARS-CoV-2 using inactivated viruses and clinical specimens.** **a**, End-point fluorescence spectra detection. **b**, Real-time amplification curves in plasmonic RT-qPCR runs. **c**, Ct values for N1 and RP, demonstrating detection down to 4,425 copies per millilitre ( $n = 3$  replicates/concentration). For N1, all concentrations were statistically significant from saliva no template control (NTC) and buffer NTC samples ( $p < 0.0001$ ), and all significant from each other except for 17,750 copies per millilitre vs 8,850 copies per millilitre which is only a two-fold instead of a ten-fold dilution. **d**, Ct values for N1, N2 and RP targets for additional concentrations ( $n = 3$  replicates/concentration). The lowest concentration detected was 2,212 copies per millilitre. For COVID targets, one-way ANOVA followed by Tukey's multiple comparisons showed 8,850 copies per millilitre, 4,425 copies per millilitre, and 2,212 copies per millilitre were all statistically significant from the saliva NTC. **e**, N1 Ct values from prototype runs versus QuantStudio (QS) ( $n = 3$  replicates/concentration). **f**, Clinical saliva specimen testing for ten positive and nine negative specimens, showing 100% sensitivity and 100% specificity. **g**, Receiver operating characteristic (ROC) curve for specimens tested in **f**. **h**, Comparison of N1 Ct values from instrument versus QuantStudio. **i**, Clinical nasal specimen testing for 20 positive and 29 negative specimens for target N1, showing 100% sensitivity and 100% specificity. **j**, ROC curve for specimens tested in **i**. **k**, Comparison of N1 Ct values for nasal clinical specimens tested with plasmonic versus QuantStudio. **l**, Clinical nasal specimen testing for 20 positive and 29 negative samples for target N-gene, showing 100% sensitivity and 100% specificity. **m**, ROC curve for specimens tested in **l**. **n**, Comparison of N-gene Ct values for nasal clinical specimens tested with plasmonic versus QuantStudio. **o**, Standard curve plotting N1 Ct values for serial dilutions of a clinical specimen (Extended Data Fig. 4). LoD of less than  $10^4$  copies per millilitre was obtained for all the three specimens. **p**, Serial dilutions for the B.1.1.7 variant run on the plasmonic instrument, with an LoD of 2,350 copies per millilitre ( $n = 3$  replicates/concentration). **q**, No cross-reactivity detected for N1 and N2 probes tested against MERS ( $n = 23$ ) and human coronavirus NL63 ( $n = 27$ ). Data for all the figures with error bars are presented as mean  $\pm$  s.d. Supplementary Information provides more details of each panel.



bins (for example, five cycles per bin or cutoff threshold values<sup>31,32</sup>) to present different viral loads that correlated with the severity of COVID-19 disease; here recognizing that there are offsets in Ct

values across different PCR setups, the samples testing low in the plasmonic RT-qPCR (for example, Ct < 33) also test low with the laboratory-based PCR (for example, Ct < 30).

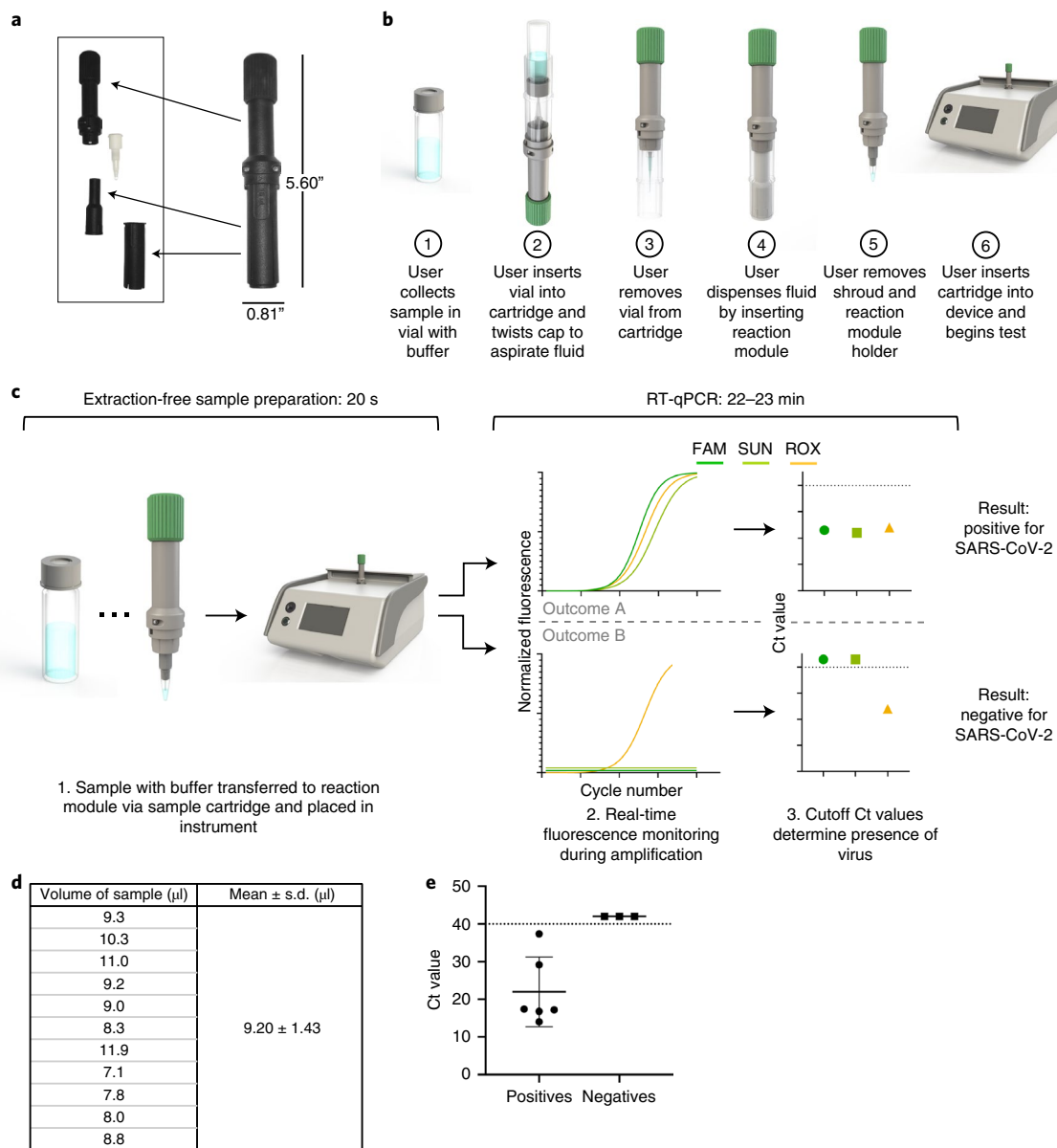


**Fig. 5 | Sample-to-result workflow, using sample cartridge for extraction-free sample preparation, followed by plasmonic thermocycling integrated with real-time multispectral fluorescence monitoring.** **a**, Image of a custom sample cartridge (entire cartridge is 5.60 in.  $\times$  0.81 in.). Disassembled components of the cartridge are shown, including the body, reaction module, plunger and shroud. **b**, Pre-analytical workflow for measuring out 10  $\mu$ l specimens using a custom sample cartridge. Renderings drafted in SOLIDWORKS. **c**, Sample-to-result process for extraction-free sample preparation and plasmonic thermocycling with real-time multispectral fluorescence monitoring. Samples with the buffer are transferred via the sample cartridge to the instrument (step 1). Multispectral fluorescence values against cycle number (step 2) are used to calculate the Ct values for the targets (N1 and N2 primers detect SARS-CoV-2 virus and RP is the human control) and determine the result (step 3). **d**, Precision of measuring across 11 different cartridges achieved an average dispense volume of  $9.2 \pm 1.4 \mu\text{l}$ . **e**, Classification of positives and negatives from our setup compared with laboratory-based PCR using clinical saliva specimens, and quantitation of Ct values for SARS-CoV-2-positive and SARS-CoV-2-negative specimens. Data are presented as mean  $\pm$  s.d.

To further illustrate the versatility and broad applicability of this approach, in addition to the saliva data collected, we tested 49 human clinical specimens collected nasally (20 positives and 29 negatives) on the integrated setup with plasmonic thermocycling and real-time fluorescence monitoring. The runs took  $24.1 \pm 0.9$  min. Two COVID targets were simultaneously detected in the same tube: N1 and N-gene. The setup yielded a sensitivity of 100% and specificity of 100% (Fig. 4i,l), and an area under the curve of 1 for both COVID targets (Fig. 4j,m) compared with a reference of laboratory-based PCR. We also evaluated the quantitative capability of the setup. The Ct values for N1 and N-gene obtained in this

setup exhibited a coefficient of determination of 0.9960 and 0.9600, respectively, compared with the Ct values of the same samples run on a laboratory-based PCR instrument (Fig. 4k,n).

Moreover, we performed serial dilutions of three clinical specimens, created a standard curve relating Ct value to concentration and determined an LoD of less than  $10^4$  viral copies per millilitre for all the three specimens (Fig. 4o and Extended Data Fig. 4b–e), similar to that measured from spiked viruses. This observation was consistent with the estimation of viral loads in the clinical specimens from Fig. 4f–h; these measurements showed that the previous quantification took place across a wide range of concentrations,

between  $10^3$  and  $10^6$  copies per millilitre for saliva specimens and  $10^4$  and  $10^9$  copies per millilitre for nasal specimens (Extended Data Fig. 5).

Much of the previous data (Fig. 4a–e) were tested on the USA-WA1/2020 strain. To assess the effectiveness of our technique for another variant, we also performed testing with SARS-CoV-2 B.1.1.7 (Alpha) variant. The data showed the detection of N1 down to 2,350 copies per millilitre of spiked B.1.1.7 virus (Fig. 4p), which closely replicates the previously demonstrated LoD, therefore showing success with two different variants.

To evaluate whether this approach could distinguish between SARS-CoV-2 and closely related viruses, we tested whether our method would detect the Middle East respiratory syndrome (MERS) and human coronavirus NL63, which are considered ‘high-priority pathogens from the same genetic family’ as SARS-CoV-2 with relatively high degrees of homology<sup>33</sup>. As expected, out of the 23 MERS replicates and 27 NL63 replicates, all of them tested at a high concentration of  $1.9 \times 10^6$  copies per millilitre and yielded a positive human RP control, and none resulted in amplification for N1 or N2 (Fig. 4q).

**Sample-to-result workflow for POC applications.** Finally, for the COVID-19 application, we noted that the extraction-free processing of human saliva specimens as input into plasmonic RT-qPCR could potentially result in a simple workflow when considered more broadly from sample collection to result. We tested this entire sample-to-result workflow, using a custom-designed cartridge that metres out saliva specimens followed by operation of the integrated plasmonic RT-qPCR instrument (Fig. 5 and Supplementary Video 1) (in previous studies of plasmonic thermocycling, clinical specimens were generally not tested; in another study without real-time fluorescence monitoring, an RNA extraction cartridge was separately tested but not together with thermocycling clinical samples from sample to result<sup>22</sup>). First, we verified the ability of the sample cartridge to dispense consistent volumes of water, showing a precision of  $9.2 \pm 1.4 \mu\text{l}$  ( $n=11$ ) (Fig. 5d). Next, we tested nine human saliva specimens (six positives and three negatives) in a full workflow from sample to result. The time from sample to result was 22–23 min, and the setup exhibited a sensitivity of 100% and specificity of 100% compared with a reference of laboratory-based PCR (Fig. 5e).

## Conclusions

For over three decades and during the COVID-19 pandemic, PCR methods have remained the indisputable gold-standard technique for clinical diagnostics. However, its use has still been limited in POC settings<sup>34</sup>. As an alternative to traditional thermocyclers, which rely on bulky heat blocks, plasmonic thermocycling provides a miniaturizable path for driving thermocycling, but previous work did not demonstrate the qPCR capability—the most commonly performed version of PCR in clinical diagnostics—on clinical specimens. Although fluorescence quenching by nanoparticles dampens the overall fluorescence signal, this work demonstrates that under appropriate nanoparticle concentrations and conditions, a real-time, accurate and multiplexed fluorescence reading can be achieved with a spectrometer with a single-wavelength light source, followed by deconvolution of the mixed fluorescence spectra. This approach—based on a combination of nanomaterial selection, instrument setup and deconvolution software—enabled RT-qPCR capability for detecting RNA copies of SARS-CoV-2 from human clinical specimens, collected either as saliva or nasally, at clinically relevant sensitivities, and with quantitative capabilities. We demonstrated a sample-to-result time of 22–23 min, including sample preparation, and an LoD of 2.2–4.4 copies per microlitre, which was competitive with other methods (for example, a study with plasmonic thermocycling<sup>22</sup> demonstrated a time to detection

of 17 min, excluding sample preparation, with an LoD of 3.2 copies per microlitre, although other studies<sup>35</sup> have demonstrated 1 min thermocycling for the PCR portion on targets in buffer). By the use of compact optical components for plasmonic thermocycling, the method was fast and miniaturizable for POC use. Our instrument showed no cross-reactivity with other viruses in the same genetic family, and worked robustly for two different SARS-CoV-2 strains. Moreover, the N1 primer and probe used in this work has been demonstrated to successfully detect other variants, including Omicron<sup>36</sup> and Delta<sup>37</sup>; in the future, standard *in silico* analysis, as per United States Food and Drug Administration (US FDA) guidelines<sup>33</sup>, can be used to prepare PCR primers for future variants.

This demonstration of plasmonic RT-qPCR holds multiple advantages for the diagnosis of COVID-19 and other infectious diseases compared with previous work. First, since fluorescence measurements do not require AuNRs to be removed from the vessel, concerns for biosafety for the user at a POC setting are reduced. Second, real-time monitoring could give early indication for strongly positive specimens with low Ct values<sup>12</sup>. Third, Ct values are widely analysed in clinical diagnostics; although not yet conclusive for COVID-19 (ref. <sup>38</sup>), there is strongly suggestive evidence that Ct values correlate with severity (for example, patients with severe COVID-19 tend to have a high viral load and a long virus-shedding period, pointing to the utility of viral load for assessing disease severity and prognosis<sup>31,39,40</sup>). Fourth, the ability to monitor and detect more than one viral target in addition to a human control target (a previous study with plasmonic thermocycling demonstrated one total target of DNA in buffer<sup>16</sup>) is of increasing relevance for detecting SARS-CoV-2 variants. Fifth, a demonstration of integrated sample-to-result workflow (versus separate cartridge and analytical steps<sup>22</sup>) further highlights the potential of plasmonic thermocycling for real clinical utility. Moreover, because of the potential shortage of RNA extraction reagents, extraction-free methods that avoid purification could be advantageous<sup>25,26</sup>; this study demonstrates plasmonic RT-PCR on clinical specimens from sample collection to result, with a workflow that takes advantage of the weak spot in the lipid bilayer<sup>41</sup> like other extraction-free saliva demonstrations<sup>25–28</sup>. To facilitate the rapid processing of multiple samples, the instruments can be stacked in a compact manner (Extended Data Fig. 6) to provide fast individualized results in high-traffic situations. Overall, the quantitation and multiplexing capabilities of this study closes the gap between the plasmonic thermocycling method and qPCR capabilities performed by current clinical diagnostic methods, and achieves this via an all-optics approach that could be offered in a POC format and with rapid thermocycling. Future work could include an expanded demonstration on a large set of patient samples suitable for clinical-level validation.

## Online content

Any methods, additional references, Nature Research reporting summaries, source data, extended data, supplementary information, acknowledgements, peer review information; details of author contributions and competing interests; and statements of data and code availability are available at <https://doi.org/10.1038/s41565-022-01175-4>.

Received: 10 June 2021; Accepted: 9 June 2022;  
Published online: 25 July 2022

## References

1. Mullis, K. et al. *Cold Spring Harbor Symposia on Quantitative Biology* Vol. 51, 263–273 (Cold Spring Harbor Laboratory Press, 1986).
2. Yang, S. & Rothman, R. E. PCR-based diagnostics for infectious diseases: uses, limitations, and future applications in acute-care settings. *Lancet Infect Dis.* **4**, 337–348 (2004).
3. Linz, U. Thermocycler temperature variation invalidates PCR results. *BioTechniques* **9**, 290–293 (1990). 286, 288.

4. Schoder, D. et al. Physical characteristics of six new thermocyclers. *Clin. Chem.* **49**, 960–963 (2003).
5. Schoder, D. et al. Novel approach for assessing performance of PCR cyclers used for diagnostic testing. *J. Clin. Microbiol.* **43**, 2724–2728 (2005).
6. Zhu, H. et al. The vision of point-of-care PCR tests for the COVID-19 pandemic and beyond. *Trends Anal. Chem.* **130**, 115984 (2020).
7. Lagally, E. T., Simpson, P. C. & Mathies, R. A. Monolithic integrated microfluidic DNA amplification and capillary electrophoresis analysis system. *Sens. Actuators B* **63**, 138–146 (2000).
8. Hoehl, S. et al. Evidence of SARS-CoV-2 infection in returning travelers from Wuhan, China. *N. Engl. J. Med.* **382**, 1278–1280 (2020).
9. Zhu, N. et al. A novel coronavirus from patients with pneumonia in China, 2019. *New Engl. J. Med.* (2020).
10. Budd, J. et al. Digital technologies in the public-health response to COVID-19. *Nat. Med.* **26**, 1183–1192 (2020).
11. Harpaldas, H. et al. Point-of-care diagnostics: recent developments in a pandemic age. *Lab Chip* **21**, 4517–4548 (2021).
12. Espy, M. et al. Real-time PCR in clinical microbiology: applications for routine laboratory testing. *Clin. Microbiol. Rev.* **19**, 165–256 (2006).
13. Richardson, H. H., Carlson, M. T., Tandler, P. J., Hernandez, P. & Govorov, A. O. Experimental and theoretical studies of light-to-heat conversion and collective heating effects in metal nanoparticle solutions. *Nano Lett.* **9**, 1139–1146 (2009).
14. Huang, X. & El-Sayed, M. A. Gold nanoparticles: optical properties and implementations in cancer diagnosis and photothermal therapy. *J. Adv. Res.* **1**, 13–28 (2010).
15. Rastinehad, A. R. et al. Gold nanoshell-localized photothermal ablation of prostate tumors in a clinical pilot device study. *Proc. Natl Acad. Sci. USA* **116**, 18590–18596 (2019).
16. Lee, J.-H. et al. Plasmonic photothermal gold bipyramidal nanoreactors for ultrafast real-time bioassays. *J. Am. Chem. Soc.* **139**, 8054–8057 (2017).
17. Roche, P. J. et al. Demonstration of a plasmonic thermocycler for the amplification of human androgen receptor DNA. *Analyst* **137**, 4475–4481 (2012).
18. Son, J. H. et al. Ultrafast photonic PCR. *Light Sci. Appl.* **4**, e280–e280 (2015).
19. Dymond, J. Explanatory chapter: quantitative PCR. *Methods Enzymol.* **529**, 279–289 (2013).
20. Moses, S. et al. Endpoint PCR detection of SARS-CoV-2 RNA. Preprint at *medRxiv* <https://doi.org/10.1101/2020.07.21.20158337> (2020).
21. Silva Junior, J. V. J. et al. End-point RT-PCR: a potential alternative for diagnosing coronavirus disease 2019 (COVID-19). *J. Virol. Methods* **288**, 114007 (2021).
22. Cheong, J. et al. Fast detection of SARS-CoV-2 RNA via the integration of plasmonic thermocycling and fluorescence detection in a portable device. *Nat. Biomed. Eng.* **4**, 1159–1167 (2020).
23. Tan, S. H., Allicock, O., Armstrong-Hough, M. & Wyllie, A. L. Saliva as a gold-standard sample for SARS-CoV-2 detection. *Lancet Respir. Med.* **9**, 562–564 (2021).
24. Uchehara, G., Kirk, A. G., Trifiro, M., Palioras, M. & Mohammadyousef, P. *Nano-, Bio-, Info-Tech Sensors and 3D Systems III* Vol. 109690A, 31–44 (SPIE, 2019).
25. Srivatsan, S. et al. SwabExpress: An End-to-End Protocol for Extraction-Free COVID-19 Testing. *Clin. Chem.* **68**, 143–152 (2022).
26. Smyrlaki, I. et al. Massive and rapid COVID-19 testing is feasible by extraction-free SARS-CoV-2 RT-PCR. *Nat. Commun.* **11**, 4812 (2020).
27. Ranoa, D. et al. Saliva-based molecular testing for SARS-CoV-2 that bypasses RNA extraction. Preprint at *bioRxiv* <https://doi.org/10.1101/2020.06.18.159434> (2020).
28. Nagura-Ikeda, M. et al. Clinical evaluation of self-collected saliva by quantitative reverse transcription-PCR (RT-qPCR), direct RT-qPCR, reverse transcription-loop-mediated isothermal amplification, and a rapid antigen test to diagnose COVID-19. *J. Clin. Microbiol.* **58**, e01438–20 (2020).
29. Wyllie, A. L. et al. Saliva or Nasopharyngeal Swab Specimens for Detection of SARS-CoV-2. *N. Engl. J. Med.* **383**, 1283–1286 (2020).
30. Zhu, J., Guo, J., Xu, Y. & Chen, X. Viral dynamics of SARS-CoV-2 in saliva from infected patients. *J. Infect.* **81**, e48–e50 (2020).
31. Magleby, R. et al. Impact of SARS-CoV-2 viral load on risk of intubation and mortality among hospitalized patients with coronavirus disease 2019. *Clin. Infect. Dis.* **73**, e4197–e4205 (2020).
32. Westblade, L. F. et al. SARS-CoV-2 viral load predicts mortality in patients with and without cancer who are hospitalized with COVID-19. *Cancer Cell* **38**, 661–671.e2 (2020).
33. US Food and Drug Administration (2021). *Template for Developers of Molecular Diagnostic Tests* (accessed 21 April 2022); <https://www.fda.gov/media/135900/download>
34. Feng, W. et al. Molecular diagnosis of COVID-19: challenges and research needs. *Anal. Chem.* **92**, 10196–10209 (2020).
35. Roche, P. J. et al. Real time plasmonic qPCR: how fast is ultra-fast? 30 cycles in 54 seconds. *Analyst* **142**, 1746–1755 (2017).
36. Ahmed, W. et al. Detection of the Omicron (B.1.1.529) variant of SARS-CoV-2 in aircraft wastewater. *Sci. Total Environ.* **820**, 153171 (2022).
37. Hamill, V. et al. Molecular detection of SARS-CoV-2 strains and differentiation of Delta variant strains. *Transbound. Emerg. Dis.* **1–11** (2021).
38. Service, R. One number could help reveal how infectious a COVID-19 patient is. Should test results include it? *Science* <https://doi.org/10.1126/science.abf0366> (2020).
39. Fajnzylber, J. et al. SARS-CoV-2 viral load is associated with increased disease severity and mortality. *Nat. Commun.* **11**, 5493 (2020).
40. Liu, Y. et al. Viral dynamics in mild and severe cases of COVID-19. *Lancet Infect. Dis.* **20**, 656–657 (2020).
41. Chang, C.-k., Hou, M.-H., Chang, C.-F., Hsiao, C.-D. & Huang, T.-h. The SARS coronavirus nucleocapsid protein-forms and functions. *Antivir. Res.* **103**, 39–50 (2014).

**Publisher's note** Springer Nature remains neutral with regard to jurisdictional claims in published maps and institutional affiliations.

© The Author(s), under exclusive licence to Springer Nature Limited 2022

## Methods

**Design of instrument for plasmonic thermocycling.** The integrated setup consisted of both plasmonic thermocycling and multispectral fluorometry, both of which can operate on the same reaction vessel with no moving components or steps. The plasmonic thermocycling prototype was developed with the following capabilities: (1) consistent heating via AuNRs, (2) real-time fluorescence detection and (3) compatibility with a simple sample cartridge. Briefly, a hexagonal three-dimensional printed hub was designed to contain all the optical components concentrically surrounding the PCR tube. Three IR LEDs, arranged in a hexagon-like manner, were aimed at the PCR tube. Each LED was positioned underneath a lens and on top of a custom-machined heat sink and fan to prevent overheating. An additional 12 V fan was positioned near the PCR tube and used to cool the sample. An airflow chamber was cut out of the bottom of the three-dimensional printed hub to ensure airflow over the PCR tube. The fluorometer components (Fig. 1c, laser and spectrometer setup) were positioned in the remaining sides of the hub and connected to an Arduino Mega board. The fluorometer was designed to comprise a 488 nm laser diode as the excitation source, with light passing through a collimating lens and bandpass filter before entering the PCR tube. The light emitted by the reaction fluid is passed through a series of filters (excitation blocking, IR blocking and longpass filtering) and a condensing lens and is then collected into a 600- $\mu$ m-diameter optical fibre, and measured by a spectrometer (Ibsen). An annotated image of the prototype (Extended Data Fig. 1) further demonstrates the hexagonal positioning of the components, and a wiring diagram (Extended Data Fig. 2) details the electronic connections used.

**Reaction conditions.** Functionalized silica-coated AuNRs were purchased from Nanopartz. AuNRs had a surface plasmon resonance peak of  $\sim$ 850 nm (slight variation between batches) and an aspect ratio of  $\sim$ 4.5 nm. A 10 nm silica coating was used to prevent the adsorption of proteins during the PCR reaction. Unless otherwise noted, the reaction conditions were as follows. PCR reactions consisted of the following: 10  $\mu$ l 2X PrimeScript III from Takara (Cat. RR600A), AuNRs (Nanopartz, final OD of 2), 500 nM forward and reverse primers (Integrated DNA Technologies), and 125 nM probes (Integrated DNA Technologies). Similar to the Centers for Disease Control and Prevention's RT-PCR test, we used the N1 and N2 primers and probes to target the SARS-CoV-2 nucleocapsid gene, and the RP primers and probes to target a human ribosomal protein (Rp) gene (Supplementary Table 3). Some reactions used an alternative nucleocapsid gene (designated 'N-gene') (Supplementary Table 3). The targets were detected using a combination of FAM, SUN, HEX and ROX fluorophores. For all the reactions on the prototypes, evaporation was prevented with Chill-out liquid wax (Bio-Rad) or mineral oil, unless otherwise noted.

Unless otherwise noted, for the plasmonic instrument, thermocycling conditions were as follows: reverse transcription for 2–5 min at 45–50 °C, followed by initial denaturation for 10–20 s at 95 °C. Next, the reaction cycled 40–45 times between a low temperature (58–60 °C) held for 0–8 s and a high temperature (91–97 °C) held for 0–1 s.

**Initial testing of amplification using plasmonic RT-PCR.** For experiments with RNA (Fig. 2), spiked RNA (BEI, Cat. NR-52285) in 1X TE buffer (10 mM Tris-HCl and 1 mM EDTA, Integrated DNA Technologies) was used to bring the reaction volume up to 20  $\mu$ l. The NTCs were tested with the same mix and conditions but without any SARS-CoV-2 RNA template, which was instead replaced with TE buffer only. Positive and negative controls were also run on a QuantStudio 6 Pro system. The prototype temperature was controlled using a K-type thermocouple for closed-loop thermal cycling conditions (Fig. 2a,b). A Python script identified the times and temperatures at which the maximum and minimum temperatures were reached and then the average heating and cooling rates were calculated for each cycle. Fluorescence measurements were made on a BioTek plate reader by aliquoting the 20  $\mu$ l post-PCR reaction to a 384-well plate, and the emission data were collected for 5-FAM, SUN and ROX dyes (measuring the amplification of SARS-CoV-2 N1, SARS-CoV-2 N2 and human RP, respectively). The LoD threshold was determined by running three NTCs and taking the mean raw fluorescence plus ten times the standard deviation (Fig. 2d, dotted line). All the concentrations were run in triplicate, except 2,960 copies per millilitre (which had six replicates). Raw fluorescence for each concentration was compared with the NTC value via one-way ANOVA followed by Sidak's multiple comparisons test.

For the experiments in Fig. 3a,b, a final concentration of OD of 18 was used for the nanoparticles. A 10  $\mu$ l PCR reaction with TaqPath ProAmp Master Mix, CG, from Thermo Fisher Scientific (Cat. A30865) was used with 500 nM forward and reverse primers (Integrated DNA Technologies) and 125 nM probes (Integrated DNA Technologies). A complementary DNA sample was thermocycled on the QuantStudio system for 20 s at 95 °C followed by 40 cycles between 95 °C (1 s) and 60 °C (2 s). After the cycles, there was a 30 s hold at 60 °C. The Ct values were determined by the QuantStudio desktop analysis software.

For the experiments in Fig. 3c–e, spiked inactivated virus (BEI, Cat. NR-52286) in 1:1 mixture of donor saliva (Innovative Research, Cat. IRHUSLS5ML) and 1X TE buffer was used to bring the reaction volume up to 20  $\mu$ l. The temperature was controlled with a thermocouple for closed-loop cycling parameters. Fluorescence

measurements on the prototype were made as follows: raw fluorescence spectra were collected by the spectrometer at the end of the annealing/extension step during each cycle. These spectra were analysed using least squares regression, based on ideal peaks experimentally determined by measuring the fluorescence spectra for amplicons containing the PCR product from a single fluorophore. Next, each component signal was plotted against the cycle number. For Fig. 3e, the fluorescence for each fluorophore was normalized by its maximum value in that run.

For Extended Data Fig. 3, a 10  $\mu$ l PCR reaction with Reliance One-Step Multiplex RT-qPCR Supermix from Bio-Rad (Cat. 12010176) and nanoparticles with a final concentration of OD of 18 was used. N1 was detected with FAM and RP was detected with HEX. The final primer concentration was 400 nM and the final probe concentration was 100 nM. Plasmonic thermal cycling conditions consisted of 1 min at 45 °C and 20 s at 95 °C, followed by 40 cycles between 54 °C (20 s) and 95 °C (0 s), as controlled by an IR pyrometer. Evaporation was prevented with 75  $\mu$ l of Chill-out PCR wax. Saliva specimens were obtained from Mirimus Foundation and SUNY Downstate from patients suspected of being infected with SARS-CoV-2 and stored at 4 °C on receipt. The samples were heat inactivated for 5 min at 95 °C before receipt. The samples were diluted at 1:1 in 1X TE buffer and added to the PCR reaction mix to reach 10  $\mu$ l. Fluorescence was measured after amplification on a BioTek plate reader.

**Characterization of heating and fluorescence quenching by AuNRs.** For the AuNR heating-rate characterization (Fig. 3f), dilutions were prepared in 1X TE buffer with AuNR concentrations ranging from OD of 0.5 to 8.0. Five samples of each concentration were thermocycled between 60 and 95 °C eight times (no holds) by a closed-loop LabVIEW program. A Python script identified the times and temperatures at which the maximum and minimum temperatures were reached and then the average heating and cooling rates were calculated for each cycle. The results are reported as the average of 40 measurements per concentration.

For the quenching characterization (Fig. 3g), dilutions were prepared in 1X TE buffer with AuNR concentrations ranging from OD of 0 to 32. An oligo with FAM attached was used as a fluorophore. For each concentration of AuNR, the concentration of FAM oligo was kept constant at 1.43  $\mu$ M. All the values are normalized to the average fluorescence measurements of the samples with OD of 0 (the brightest sample). For each concentration, three samples were measured three times each, and the data are reported as nine replicates. The optical LoD was calculated as the average plus ten times the standard deviation of stock AuNR (OD of 94).

**Evaluation of performance of plasmonic PCR.** For Fig. 4a–c,e, spiked inactivated virus (BEI, Cat. NR-52286) in 1:1 mixture of donor saliva (Innovative Research, Cat. IRHUSLS5ML) and 1X TE buffer was used to bring the reaction volume up to 20  $\mu$ l. The NTCs were tested with the same mix and conditions but without any template (inactivated SARS-CoV-2 virus). Buffer NTCs indicate the use of a TE buffer only, and saliva NTCs indicate the use of donor saliva mixed in 1:1 with the TE buffer as described below. Positive and negative controls were also run on a QuantStudio 6 Pro system. Thermocycling conditions were initially calibrated in LabVIEW using closed-loop control, and the output was converted to an open-loop format for testing. The samples were considered positive on the prototype if both N1 and RP were detected ( $C_t < 46$ ). As commonly done for diagnostic tests, samples for which human RP failed to amplify were considered indeterminate<sup>42</sup>. Onboard fluorescence measurements on the prototype were made as previously described. For Fig. 4b, N1 fluorescence was smoothed and normalized. The baseline was individually selected for each run to account for fluorometer noise. The fluorescence threshold value was calculated as the mean plus ten times the standard deviation of the baseline. The  $C_t$  value was calculated to be the interpolated cycle at which the fluorescence signal crossed the calculated threshold value. Any  $C_t$  value less than the number of cycles was interpreted as positive.

For Fig. 4d, spiked inactivated virus (BEI, Cat. NR-52286) in 1:1 mixture of donor saliva (Innovative Research, Cat. IRHUSLS5ML) and 1X TE buffer was used to bring the reaction volume up to 20  $\mu$ l. The NTCs were tested with the same mix and conditions but without any template (inactivated SARS-CoV-2 virus). Saliva NTCs indicate the use of donor saliva mixed in 1:1 with the TE buffer as described above. Positive and negative controls were also run on a QuantStudio 6 Pro system. Thermocycling conditions were initially calibrated in LabVIEW using closed-loop control, and the output was converted to an open-loop format for testing. Onboard fluorescence measurements on the prototype were made as described above. The baseline was preselected to be cycles 0–20. The fluorescence threshold value was calculated as the mean plus ten times the standard deviation of the baseline. The  $C_t$  value was calculated to be the interpolated cycle at which the fluorescence signal crossed the calculated threshold value. Any  $C_t$  value less than the number of cycles was interpreted as positive. The samples were considered positive if N1 or N2 was detected (regardless of RP detection). The LoD was determined as the lowest concentration resulting in the positive detection of at least three out of three samples, based on US FDA guidelines<sup>43</sup> and established standard of many products obtaining emergency use authorization.

**Detection of SARS-CoV-2 RNA from human clinical saliva samples.** For Fig. 4f–h, the PCR reactions were similar to those generally described above. Deidentified clinical specimens were obtained under a protocol approved by the

Columbia University Medical Center Institutional Review Board (AAAT0100). Saliva specimens were obtained from Mirimus Foundation and SUNY Downstate from patients suspected of being infected with SARS-CoV-2 and stored at 4°C on receipt. The samples were not heat inactivated. The samples were diluted at 1:1 in 1X TE buffer and added to the PCR reaction mix (as described above) to reach 20 µl.

Although all the clinical testing occurred within two weeks of receiving the samples, in light of possible sample degradation during transportation and storage, we reconfirmed the status of the specimens by running them in duplicates on laboratory-based qPCR using a Thermo Fisher QuantStudio 6 Pro instrument, which acted as our laboratory-based PCR reference (consistent with previous studies using established RT-qPCR methods to measure SARS-CoV-2 RNA from human saliva specimens<sup>44,45</sup>). Positive and negative reaction controls were included on every QuantStudio plate: templates for positive control reactions contained 4,425 copies per millilitre of inactivated SARS-CoV-2 virus from nCoV 2019-nCoV/USA-WA1/2020 (BEI, Cat. NR-52286) in 7.9 µl of a single human donor saliva from Innovative Research (Cat. IRHUSLS5ML) mixed in 1:1 with 1X TE buffer from Integrated DNA Technologies (Cat. 11-01-02-02), saliva negative reaction controls contained only saliva and TE buffer, and buffer negative reaction controls only contained the buffer. Reactions were run on a QuantStudio 6 Pro real-time PCR system (Applied Biosystems) using a thermal cycling program for 2 min at 50°C, 1 min at 95°C, and 40 cycles of 2 s at 60°C and 1 s at 95°C. The Ct values were determined using the QuantStudio desktop analysis software. A sample was considered positive if N1 was detected, negative if N1 was not detected and RP was detected, and indeterminate if neither N1 nor RP was detected (Supplementary Table 4). Indeterminate samples were excluded from the analysis. Only samples for which both duplicate wells were correctly amplified (positives) or did not amplify (negatives) in QuantStudio (for laboratory-based PCR) were considered viable.

For the plasmonic instrument, thermocycling conditions were initially calibrated in LabVIEW using closed-loop control, and the output was converted to an open-loop format for testing. Fluorescence signals were collected and deconvolved as described above. The baseline was preselected to be cycles 8–18 but was modified for two samples to account for fluorescence noise. The fluorescence threshold value was calculated as the mean plus ten times the standard deviation of the baseline. The Ct value was calculated to be the interpolated cycle at which the fluorescence signal crossed the calculated threshold value. Any Ct value less than the number of cycles was interpreted as positive. The samples on the prototype were considered positive if N1 was detected ( $Ct < 46$ ) regardless of RP detection, negative if N1 was undetected and RP was detected, and indeterminate if both targets were undetected. All the clinical samples were tested once if positive or negative, and twice if indeterminate. If an indeterminate sample tested either positive or negative on repeating the run, that result was used (possibly due to variability of patient saliva and/or an opportunity to explore additional lysis reagents in the buffer, the setup initially produced 14 indeterminate results in which human Rp gene was not initially detected; although re-running the specimen produced viable results for nine samples to leave the total number of indeterminate results to five, we are working to refine the sample collection and preprocessing protocol to minimize the number of indeterminates). For all the viable samples, our results were fully concordant with the reference results from Mirimus Foundation for which the TaqPath kit (emergency use authorization by the US FDA) was used.

**Detection of SARS-CoV-2 RNA in human clinical nasal samples.** For Fig. 4i–n, deidentified clinical specimens were obtained frozen from the PATH Washington COVID-19 Biorepository (PATH, Seattle, USA), hereafter the Biorepository, and stored at 4°C after thawing. The samples tested in Fig. 4i–n underwent a 1 min heat lysis step at 95°C before testing. A 7.7 µl aliquot of undiluted clinical sample was added to each 20 µl PCR reaction. In light of possible sample degradation during transportation and storage, we confirmed the status of the specimens by running them in triplicates on laboratory-based qPCR using a Thermo Fisher QuantStudio 6 Pro instrument, which acted as our laboratory-based PCR reference. QuantStudio reactions used a thermal cycling program of 5 min at 50°C, 10 s at 95°C, and 40 cycles of 8 s at 60°C and 1 s at 95°C. Positive and negative reaction controls were included on every QuantStudio plate: templates for positive control reactions contained <5,000 copies per millilitre of inactivated SARS-CoV-2 virus from nCoV 2019-nCoV/USA-WA1/2020 (BEI, Cat. NR-52286) in 7.7 µl of 1X TE buffer from Integrated DNA Technologies (Cat. 11-01-02-02), and buffer negative reaction controls contained only buffer and Master Mix. The Ct values were determined using the QuantStudio desktop analysis software. Only samples for which all the three triplicate wells were correctly identified for both N1 and N-gene as positive or negative by QuantStudio were considered viable.

For the plasmonic instrument, the temperatures were controlled using closed-loop sensing with a wire thermocouple, and thermal cycling conditions were programmed in LabVIEW. The Ct values were called using a custom Python script, which identified the fractional cycle at which the second derivative of the fluorescence signal was at its maximum, a method that has been previously validated<sup>46</sup>. Any Ct value less than the number of cycles was interpreted as positive. A sample was considered positive if N1 or N-gene was detected (regardless of RP detection); negative if neither N1 nor N-gene was detected and RP was detected;

and indeterminate if N1, N-gene and RP were not detected (Supplementary Table 5). The samples were tested once if positive or negative, and twice if indeterminate. If an indeterminate sample tested either positive or negative on repeating the run, that result was used. If a sample tested indeterminate a second time on repeating the run, it was excluded from the analysis. Only three samples had indeterminate results. Re-running the samples produced viable results for one of the specimens, leaving the final number of indeterminate samples at two. All the viable samples were concordant with disease status reported from the Biorepository.

**Detection of SARS-CoV-2 RNA in diluted human clinical nasal samples.** For a subset of samples (Fig. 4o and Extended Data Fig. 4b–e), the QuantStudio Ct value was used to estimate the viral load based on a spiked-virus standard curve. These clinical samples were then diluted in TE buffer to the desired estimated concentration and tested on the plasmonic instrument three times per dilution.

Deidentified clinical specimens were obtained frozen from the Biorepository and stored at 4°C after thawing. The samples tested in Fig. 4o and Extended Data Fig. 4b–e underwent a 1 min heat lysis step at 95°C before testing. A 7.5 µl aliquot of undiluted, lysed clinical sample was added to a 20 µl PCR reaction. We first tested the specimens in triplicate on laboratory-based qPCR using a Thermo Fisher QuantStudio 6 Pro instrument. The clinical samples were concurrently run on QuantStudio with a full standard curve, which ranged from 1.8 million copies per millilitre to <5,000 copies per millilitre of heat-inactivated SARS-CoV-2 USA/CA\_CDC\_5574/2020 (BEI, Cat. NR-55245) spiked into 1X TE buffer. The Ct values were determined using the QuantStudio desktop analysis software.

To determine the viral load of the clinical samples, we first used the spiked-virus serial dilution to correlate the QuantStudio Ct value with the concentration of the spiked virus. A log-plot of the QuantStudio Ct values versus concentration of spiked virus was generated in GraphPad Prism and a linear regression equation was fit to the data (Extended Data Fig. 4a). The Ct values from the clinical samples were then translated into estimated viral concentrations based on the regression equation (Fig. 4o and Extended Data Figs. 4 and 5). Concentrations for diluted samples (Fig. 4o and Extended Data Fig. 4b–e) were calculated based on the estimated raw-sample viral concentrations.

From the estimated clinical-sample viral concentrations, we sought to determine whether our device could detect down to the same LoD of virus in clinical samples as we had previously shown with the spiked virus. To do this, we tested the serial dilutions of clinical samples on our plasmonic instrument. The temperatures were controlled using closed-loop sensing with a wire thermocouple, and thermal cycling conditions were programmed in LabVIEW. To quantify the amplification, the fluorescence threshold was calculated as the mean plus ten times the standard deviation of the average of the baseline, which was predetermined to be cycles 11–23. The Ct value was calculated to be the interpolated cycle at which the fluorescence signal crossed the calculated threshold value. Any Ct value less than the number of cycles was interpreted as positive. A sample was considered positive if N1 or N2 was detected (regardless of RP detection); negative if neither N1 nor N2 was detected and RP was detected; and indeterminate if N1, N2 and RP were not detected (Supplementary Table 5). Indeterminate runs were excluded from the analysis.

The clinical-sample serial dilutions were used to create a plasmonic-instrument standard curve (Fig. 4o and Extended Data Fig. 4c–e) with a regression equation fit to the data in GraphPad Prism.

**Specificity testing with viruses closely related to SARS-CoV-2.** To evaluate whether our assay could distinguish between SARS-CoV-2 and closely related viruses, we tested higher concentrations of MERS coronavirus (BEI, Cat. NR-50171) and human coronavirus NL63 (BEI, Cat. NR-53530) (Fig. 4q).

Heat-inactivated virus (MERS or NL63) was diluted to approximately 1,875,000 copies per millilitre in TE buffer. Then, 7.5 µl of the diluted virus was added to each 20 µl PCR reaction. Each reaction also had spiked total RNA control (Human) (Thermo Fisher, Cat. 4307281) at a concentration of 0.1875 ng µl<sup>-1</sup> for RP detection as a sample-processing control. The samples were tested on the plasmonic instrument using closed-loop sensing with a wire thermocouple, and thermal cycling conditions were programmed in LabVIEW. To quantify the amplification, the fluorescence threshold was calculated as the mean plus ten times the standard deviation of the baseline (cycles 11–23). The Ct value was calculated to be the interpolated cycle at which the fluorescence signal crossed the calculated threshold value. Any Ct value less than the number of cycles was interpreted as positive. A sample was considered positive if N1 or N2 was detected (regardless of RP detection); negative if neither N1 nor N2 was detected and RP was detected; and indeterminate if N1, N2 and RP were not detected (Supplementary Table 5). Indeterminate runs were excluded from the analysis.

**Sample cartridge for sample-to-result workflow.** We designed a sample cartridge that was simple to use and measured out a preset quantity (10 µl) of the specimen into the PCR tube (Fig. 5). This design features a twist cap to aspirate a designated volume of the solution, and a push-to-dispense feature to eject ~10 µl fluid into the reaction mix without allowing for potential sample exposure to the operator (Fig. 5a). First, the user collects approximately 500 µl of saliva into a tube prefilled with 500 µl of 1X TE buffer to achieve 1:1 dilution (~1 min) (dilution of

specimen with plain buffer followed by the direct amplification of crude lysate, with no separate step for RNA extraction, has been shown to previously work for nasopharyngeal swabs<sup>25</sup>; future work on the use of alternate single-step buffers that can lyse host cells in saliva specimens is needed to improve the results). Second, a custom-designed sample cartridge is used to measure 10 µl of the specimen into a PCR tube containing Master Mix (primers, nucleotides, enzymes and AuNRs, as described above) (20 s) (Fig. 5b and Supplementary Video 1). We used a one-step RT-PCR mix (described above) for a single reaction. Third, the user inserts the PCR tube into the reaction module, removes the reaction module holder, inserts the cartridge into the device and starts thermocycling. The cartridge itself sits passively and plays no other role once inserted; it is removed at the end of the test. As in laboratory-based real-time PCR, the measurements are taken after each cycle, and multispectral fluorescence is computed over the duration of 45 cycles. A test result is determined by comparing the Ct values to previously defined thresholds. Including sample preparation steps, our workflow from sample collection to test result consists of three steps from a user and takes place in 22–23 min (Fig. 5c).

For Fig. 5e, Master Mix, AuNR and clinical samples were the same, as described above (Fig. 4f–h). The thermocycling conditions were initially calibrated in LabVIEW using closed-loop control, and the output was converted to an open-loop format for testing. The fluorescence collection and Ct value interpretation were the same as described for Fig. 4f–h, except that the baseline was preselected to be cycles 5–25 for all the samples. The samples that were indeterminate were not retested due to a limited number of cartridges.

Overall, the cost of goods for a test kit, which included the materials and reagents in the sample cartridge and PCR tube, was less than US \$10 at scale.

**Statistics.** All the statistics, including one-way ANOVA followed by Sidak's multiple comparison tests and one-way ANOVA followed by Tukey's multiple comparison tests, were performed using GraphPad Prism 9 software.

**Informed consent.** The PATH Washington COVID-19 Biorepository (PATH, Seattle, USA) is a specimen biorepository that was constructed by adhering to a governance plan with oversight and approval from PATH Legal Services and the PATH Office of Regulatory Affairs to ensure ethical compliance. The nasal eluate samples obtained from the Biorepository were deidentified clinical discard specimens acquired from CLIA registered laboratories that were testing for SARS-CoV-2 using US FDA EUA RT-PCR assays. The clinical saliva samples were deidentified clinical discard specimens obtained from the Mirimus Foundation with patient consent. Both sources of samples were tested in adherence to US FDA guidelines.

**Reporting summary.** Further information on research design is available in the Nature Research Reporting Summary linked to this article.

## Data availability

Source data are provided with this paper. The data that support the findings of this study are available from the corresponding author upon reasonable request; release of clinical data is subject to approval from the Institutional Review Board at Columbia University Medical Center.

## Code availability

The code designed for data collection and analysis of this study is available from the corresponding author upon reasonable request.

## References

42. Orig3n, Inc. *Accelerated Emergency Use Authorization (EUA) Summary Orig3n 2019 Novel Coronavirus (COVID-19) Test (Orig3n, Inc.). Orig3n 2019 Novel Coronavirus (COVID-19) Test EUA Summary* <https://www.fda.gov/media/136873/download> (2020).
43. US Food and Drug Administration (2022). *In Vitro Diagnostics EUAs* (accessed 21 April 2022); <https://www.fda.gov/medical-devices/coronavirus-disease-2019-covid-19-emergency-use-authorizations-medical-devices-vitro-diagnostics-euas>
44. Huber, M. et al. High efficacy of saliva in detecting SARS-CoV-2 by RT-PCR in adults and children. *Microorganisms* **9**, 642 (2021).
45. Winnett, A. et al. SARS-CoV-2 viral load in saliva rises gradually and to moderate levels in some humans. Preprint at *medRxiv* <https://doi.org/10.1101/2020.12.09.20239467> (2020).
46. Luu-The, V., Paquet, N., Calvo, E. & Cumps, J. Improved real-time RT-PCR method for high-throughput measurements using second derivative calculation and double correction. *BioTechniques* **38**, 287–293 (2005).

## Acknowledgements

This work was supported by a gift from B. Zhao, and the NIH Rapid Acceleration of Diagnostics (RADx) Tech program as funded in whole or in part with federal funds from the National Heart, Lung and Blood Institute; National Institute of Biomedical Imaging and Bioengineering; National Institutes of Health, Department of Health and Human Services, under grant no. U54HL143541. The following reagents were deposited by the Centers for Disease Control and Prevention and obtained through BEI Resources, NIAID, NIH: Genomic RNA from SARS-Related Coronavirus 2, Isolate USA-WA1/2020, NR-52285; SARS-Related Coronavirus 2, Isolate USA-WA1/2020, Heat-Inactivated, NR-52286. Figure 1a–c was created with BioRender (<https://biorender.com/>).

## Author contributions

N.R.B., M.A.E.B., M.J., M.F. and S.K.S. designed the experiments. N.R.B., M.A.E.B., J.F., N.S., J.R., A.G.A. and X.L. ran the assays. N.R.B., M.A.E.B., M.J., S.Z., J.F., Y.H., G.S.T., and T.L.C. built the instruments. N.R.B., A.M.T., Y.H., A. Sekhar, A. Sanogo, R.K., K.H. and K.M. worked on the sample cartridge. N.R.B., M.A.E.B., M.J., S.Z., J.F., T.L.C., B.O. and V.B. worked on the fluorometer. N.R.B., M.A.E.B., M.J. and A.G.A. performed the data analysis. N.R.B., M.A.E.B., A.G.A. and S.K.S. wrote the manuscript.

## Competing interests

Authors with affiliation to Rover Diagnostics, and S.K.S., had or have financial interest in Rover Diagnostics. All other authors declare no competing interests.

## Additional information

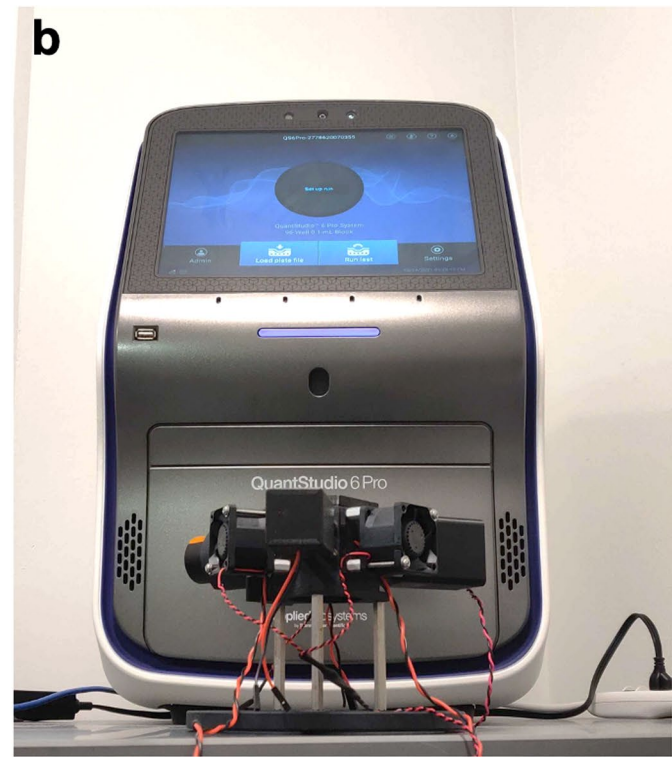
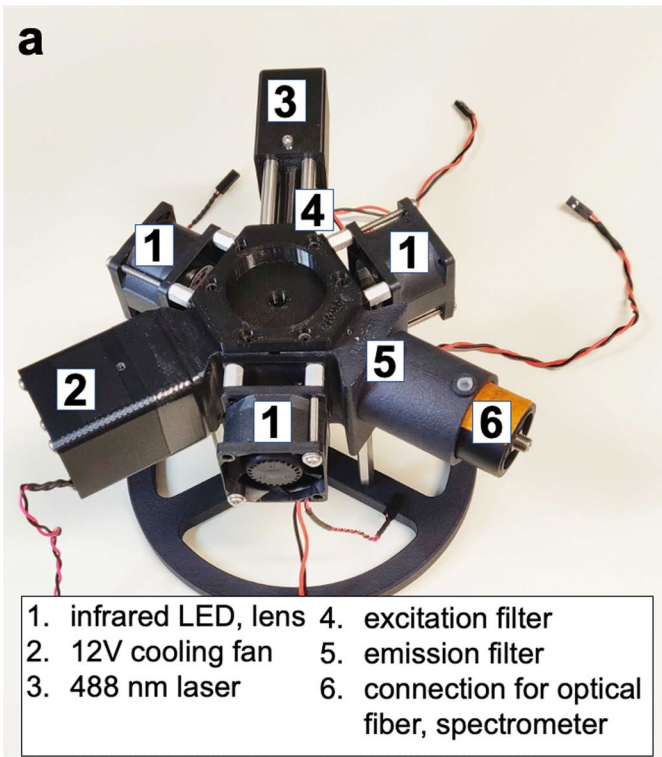
Extended data is available for this paper at <https://doi.org/10.1038/s41565-022-01175-4>.

Supplementary information The online version contains supplementary material available at <https://doi.org/10.1038/s41565-022-01175-4>.

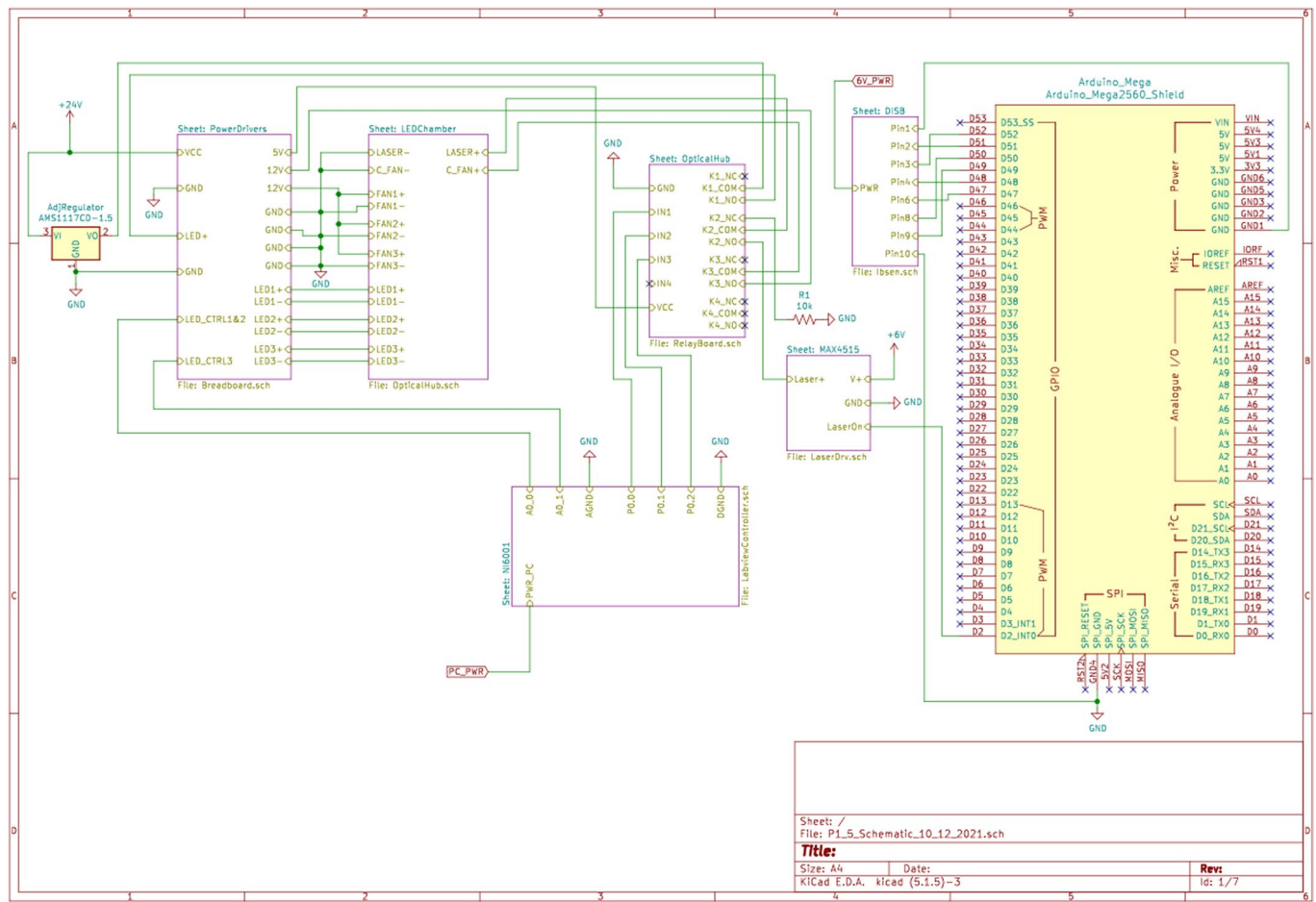
Correspondence and requests for materials should be addressed to Samuel K. Sia.

Peer review information *Nature Nanotechnology* thanks Chuen-Yen Lau and the other, anonymous, reviewer(s) for their contribution to the peer review of this work.

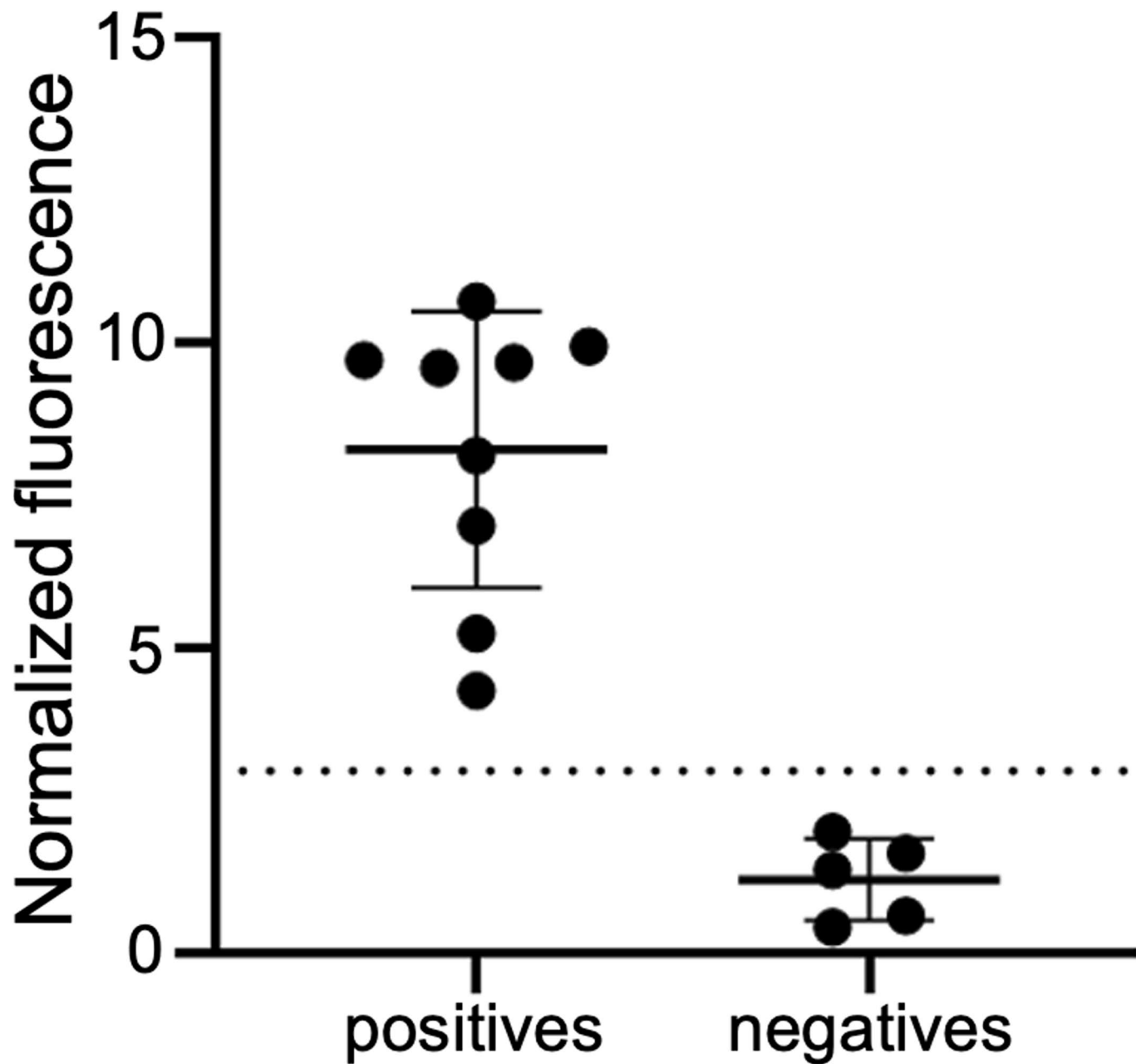
Reprints and permissions information is available at [www.nature.com/reprints](http://www.nature.com/reprints).



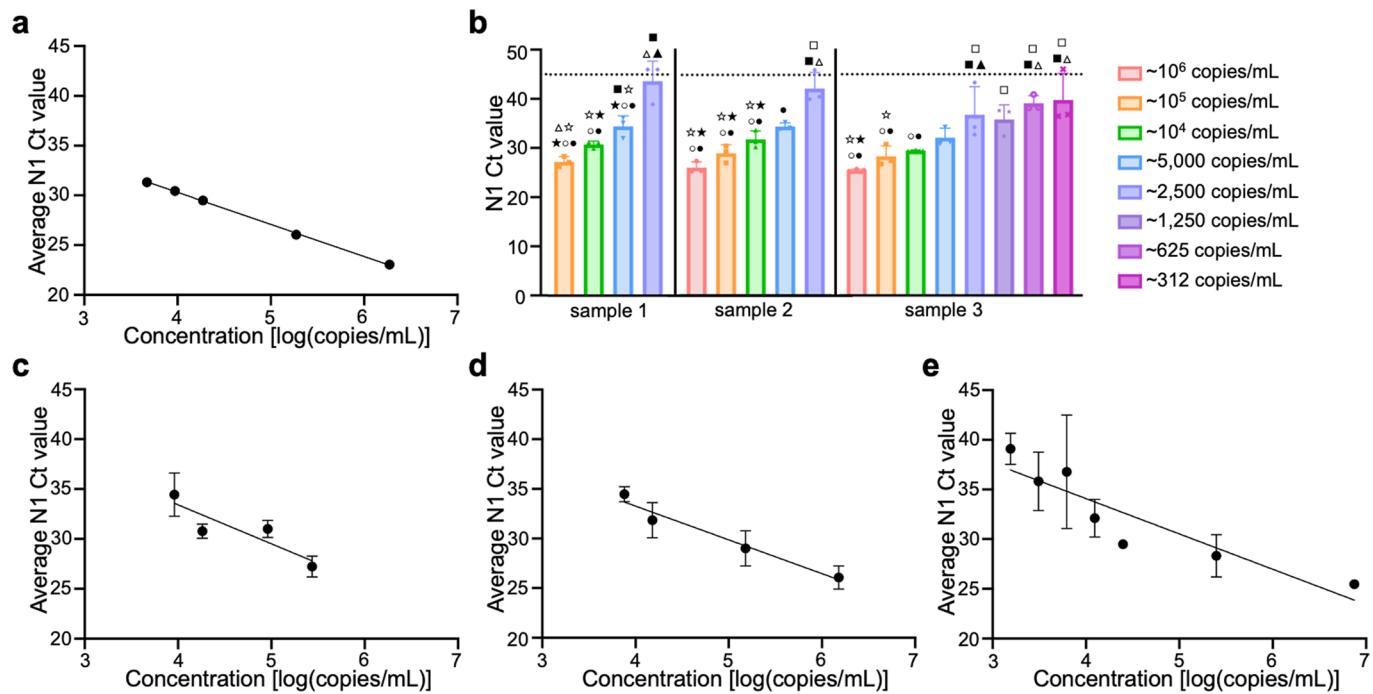
**Extended Data Fig. 1 | Image of instrument and optical setup.** **(a)** Core instrumentation with labeled components. Modular hexagon in center forms base to attach components and hold test sample in center. Circuit attachments and outer casing not shown. **(b)** Size comparison of our RT-qPCR system with a lab-based qPCR instrument (QuantStudio).



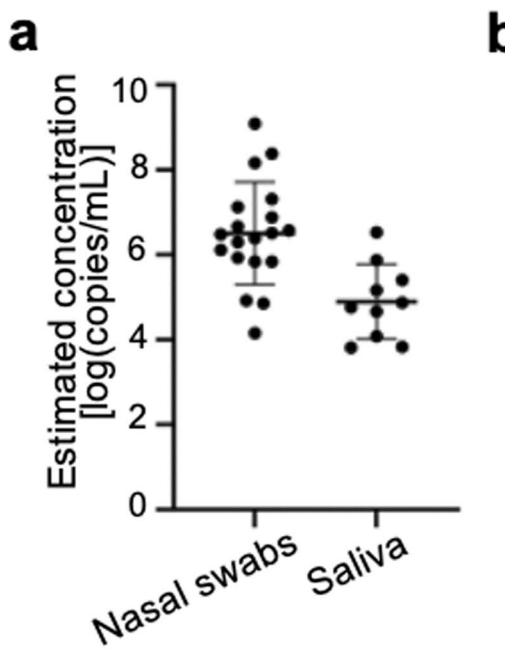
**Extended Data Fig. 2 | Wiring diagram for system circuitry.** Diagram depicting connections between key electrical components (IR LEDs, fans, laser, and spectrometer) and their controllers. Parts comprise a mix of commercially available controllers (National Instruments, Arduino) and custom soldered circuit boards. The system is powered by a 24 V power supply.



**Extended Data Fig. 3 | Testing of human saliva samples for SARS-CoV-2 to validate an extraction-free workflow with plasmonic thermocycling.** In this setup, the plasmonic thermocycling featured 2 LEDs and AuNRs at a concentration of OD 18. Fluorescence was read by a plate reader ( $n=9$  positives,  $n=5$  negatives). Data are presented as mean values  $\pm$  SD.



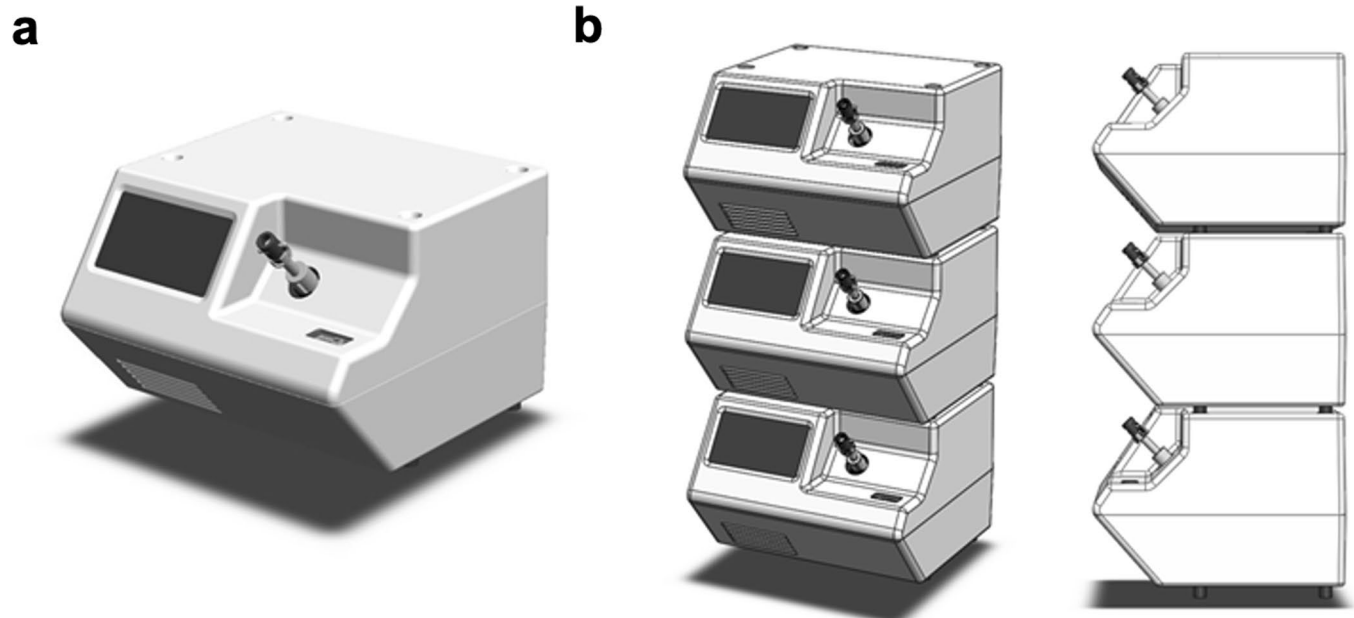
**Extended Data Fig. 4 | Serial dilutions and standard curves of 3 clinical specimens.** (a) Standard curve relating Ct value to spiked virus concentration, averaged across 3 replicates on a standard method (QuantStudio). This standard curve was used to calculate concentrations of the clinical specimens. Standard deviation error bars present but not visible due to small range. Slope was -3.22. (b) N1 Ct values for serial dilutions of three different clinical specimens. Limit of detection (lowest concentration with 3/3 replicates detected below threshold) of less than  $10^4$  copies/mL was obtained for all 3 specimens. Data are presented as mean values  $\pm$  SD. Threshold was set at 45 cycles, and samples that were not detected during amplification were plotted as having Ct values of 46. Concentrations are approximated in legend; sample 1 exact starting concentration was 273,771 copies/mL, sample 2 exact starting concentration was 1,521,025 copies/mL, and sample 3 exact starting concentration was 7,470,693 copies/mL. Symbols indicate statistical significance for the following comparisons:  $\square$  against  $\sim 10^6$  copies/mL,  $\blacksquare$  against  $\sim 10^5$  copies/mL,  $\triangle$  against  $\sim 10^4$  copies/mL,  $\blacktriangle$  against  $\sim 5,000$  copies/mL,  $\star$  against  $\sim 2,500$  copies/mL,  $\star$  against  $\sim 1,250$  copies/mL,  $\circ$  against  $\sim 625$  copies/mL,  $\bullet$  against  $\sim 312$  copies/mL. (c-e) Three separate standard curves relating Ct value to viral concentration from dilution series from three different clinical specimens. Data shown are averaged across 3 replicates run on the plasmonic instrument, presented as mean values  $\pm$  SD. The slopes of the three separate dilution series were -3.40 (d), -3.56 (e), and -3.91 (c), corresponding to acceptable amplification efficiencies (that is high efficiencies of  $>90\%$  for (d) and (e), and still  $>80\%$  for (c)), consistent with the demonstrated high sensitivity and specificity of the method on clinical specimens.



**b**

Estimated Viral Load (copies/mL)	
Nasal swabs	Saliva
1,216,746,204.0	3,350,078.63
240,275,782.34	748,376.26
146,656,055.5	250,628.24
20,354,479.4	145,039.07
13,331,530.17	74,386.65
7,582,981.6	57,193.94
4,628,390.6	45,242.33
3,745,760.45	12,156.82
3,252,969.6	6,693.91
3,031,447.1	6,460.33
2,453,352.77	
1,985,500.50	
1,300,439.0	
851,745.8	
689,318.60	
689,318.60	
83,084.5	
72,153.9	
14,248.53	

**Extended Data Fig. 5 | Measurement of viral load of clinical specimens.** Estimated concentration based on QS N1 Ct value shows wide range for both nasal (n=19) and saliva (n=10) specimens. Data are presented as mean values +/- SD.



**Extended Data Fig. 6 | CAD design of stacked instruments for processing multiple specimens.** **(a)** CAD design of one form factor of the instrument is shown, with dimensions of 12" W x 8" H x 11.7" D. Disposable cartridges are placed into this instrument. **(b)** Stacked configurations of instruments for processing of multiple specimens.

## Reporting Summary

Nature Portfolio wishes to improve the reproducibility of the work that we publish. This form provides structure for consistency and transparency in reporting. For further information on Nature Portfolio policies, see our [Editorial Policies](#) and the [Editorial Policy Checklist](#).

### Statistics

For all statistical analyses, confirm that the following items are present in the figure legend, table legend, main text, or Methods section.

n/a Confirmed

- The exact sample size ( $n$ ) for each experimental group/condition, given as a discrete number and unit of measurement
- A statement on whether measurements were taken from distinct samples or whether the same sample was measured repeatedly
- The statistical test(s) used AND whether they are one- or two-sided  
*Only common tests should be described solely by name; describe more complex techniques in the Methods section.*
- A description of all covariates tested
- A description of any assumptions or corrections, such as tests of normality and adjustment for multiple comparisons
- A full description of the statistical parameters including central tendency (e.g. means) or other basic estimates (e.g. regression coefficient) AND variation (e.g. standard deviation) or associated estimates of uncertainty (e.g. confidence intervals)
- For null hypothesis testing, the test statistic (e.g.  $F$ ,  $t$ ,  $r$ ) with confidence intervals, effect sizes, degrees of freedom and  $P$  value noted  
*Give  $P$  values as exact values whenever suitable.*
- For Bayesian analysis, information on the choice of priors and Markov chain Monte Carlo settings
- For hierarchical and complex designs, identification of the appropriate level for tests and full reporting of outcomes
- Estimates of effect sizes (e.g. Cohen's  $d$ , Pearson's  $r$ ), indicating how they were calculated

*Our web collection on [statistics for biologists](#) contains articles on many of the points above.*

### Software and code

Policy information about [availability of computer code](#)

Data collection A deconvolution software assisted with taking fluorescence measurements. A custom LabView software was used to control thermal cycling for closed-loop control in initial experiments, and a corollary LabView program was written to enable open-loop control in downstream experiments.

Data analysis GraphPad Prism 9 software was used for statistical analysis.

For manuscripts utilizing custom algorithms or software that are central to the research but not yet described in published literature, software must be made available to editors and reviewers. We strongly encourage code deposition in a community repository (e.g. GitHub). See the Nature Portfolio [guidelines for submitting code & software](#) for further information.

### Data

Policy information about [availability of data](#)

All manuscripts must include a [data availability statement](#). This statement should provide the following information, where applicable:

- Accession codes, unique identifiers, or web links for publicly available datasets
- A description of any restrictions on data availability
- For clinical datasets or third party data, please ensure that the statement adheres to our [policy](#)

The data that support the findings of this study are available from the corresponding author upon reasonable request; clinical data release is subject to approval from the Institutional Review Board at Columbia University Medical Center.

## Human research participants

Policy information about [studies involving human research participants and Sex and Gender in Research](#).

### Reporting on sex and gender

All specimens were de-identified, and therefore no information on sex and gender was collected.

### Population characteristics

Saliva and nasal clinical specimens provided by participants were de-identified from the Mirimus Foundation and SUNY Downstate, and the PATH Washington COVID-19 Biorepository, respectively; therefore, the researchers were blinded and do not know the population characteristics.

### Recruitment

Saliva and nasal specimens were obtained from patients suspected of being infected with SARS-CoV-2 from the Mirimus Foundation and SUNY Downstate, and the PATH Washington COVID-19 Biorepository, respectively. Specimens were de-identified and not directly recruited by the authors.

### Ethics oversight

De-identified clinical specimens were obtained under a protocol approved by the Columbia University Medical Center IRB (AAAT0100).

Note that full information on the approval of the study protocol must also be provided in the manuscript.

## Field-specific reporting

Please select the one below that is the best fit for your research. If you are not sure, read the appropriate sections before making your selection.

Life sciences

Behavioural & social sciences

Ecological, evolutionary & environmental sciences

For a reference copy of the document with all sections, see [nature.com/documents/nr-reporting-summary-flat.pdf](https://nature.com/documents/nr-reporting-summary-flat.pdf)

## Life sciences study design

All studies must disclose on these points even when the disclosure is negative.

### Sample size

All available specimens were tested.

### Data exclusions

Samples that were determined to be indeterminate (neither N1 or RP detected) were excluded from analysis.

### Replication

Replicates were run for all samples. For saliva clinical samples, replicates were run and compared to results from Mirimus Foundation, which used an FDA EUA authorized test kit. All attempts at replication were successful, with the exception of one specimen which tested positive from the vendor but which tested negative in one well and positive in the other on the QuantStudio instrument, and negative on the plasmonic system twice.

### Randomization

Provided clinical specimens were tested randomly by researchers.

### Blinding

Positive and negative SARS-CoV-2 specimen status was provided to researchers upon receipt of specimens, but was not referenced during testing.

## Reporting for specific materials, systems and methods

We require information from authors about some types of materials, experimental systems and methods used in many studies. Here, indicate whether each material, system or method listed is relevant to your study. If you are not sure if a list item applies to your research, read the appropriate section before selecting a response.

### Materials & experimental systems

n/a	Involved in the study
<input checked="" type="checkbox"/>	<input type="checkbox"/> Antibodies
<input checked="" type="checkbox"/>	<input type="checkbox"/> Eukaryotic cell lines
<input checked="" type="checkbox"/>	<input type="checkbox"/> Palaeontology and archaeology
<input checked="" type="checkbox"/>	<input type="checkbox"/> Animals and other organisms
<input checked="" type="checkbox"/>	<input type="checkbox"/> Clinical data
<input checked="" type="checkbox"/>	<input type="checkbox"/> Dual use research of concern

### Methods

n/a	Involved in the study
<input checked="" type="checkbox"/>	<input type="checkbox"/> ChIP-seq
<input checked="" type="checkbox"/>	<input type="checkbox"/> Flow cytometry
<input checked="" type="checkbox"/>	<input type="checkbox"/> MRI-based neuroimaging